https://doi.org/10.5194/bg-2019-74
Preprint. Discussion started: 25 September 2019

Biogeosciences Discussions Open Access EGU

Shell chemistry of the Boreal Campanian bivalve *Rastellum diluvianum* (Linnaeus, 1767) reveals temperature seasonality, growth rates and life cycle of an extinct Cretaceous oyster.

Niels J. de Winter[1], Clemens V. Ullmann[2], Anne M. Sørensen[3], Nicolas R. Thibault[4], Steven Goderis[1], Stijn J.M. Van Malderen[5], Christophe Snoeck[1,6], Stijn Goolaerts[7], Frank Vanhaecke[5], Philippe Claeys[1]

[1]AMGC research group, Vrije Universiteit Brussel, Pleinlaan 2, B-1050 Brussels, Belgium.

[2]Camborne School of Mines, University of Exeter, Penryn, Cornwall, TR10 9FE, UK.

[3]Trap Danmark, Agem All 13, DK-2970, Hørsholm, Denmark.

[4] Department of Geoscience and Natural Resource Management, University of Copenhagen, Øster voldgade 10, DK-1350 Copenhagen C., Denmark.

[5]A&MS research unit, Ghent University Campus Sterre, Krijgslaan 281, Building S12, B-9000 Ghent, Belgium.

[6]G-Time laboratory, Université Libre de Bruxelles, 50 Avenue F.D. Roosevelt, B-1050, Brussels, Belgium.

[7]Directorate of Earth and History of Life, Royal Belgian Institute of Natural Sciences, Vautierstraat 29, B-1000 Brussels, Belgium.

Correspondence to: Niels J. de Winter (niels.de.winter@vub.be)

https://doi.org/10.5194/bg-2019-74
Preprint. Discussion started: 25 September 2019

Biogeosciences Discussions

Abstract

The Campanian age (Late Cretaceous) is characterized by a warm greenhouse climate with limited land ice volume. This makes the Campanian an ideal target for the study of climate dynamics during greenhouse periods, which are essential for predictions of future climate change due to anthropogenic greenhouse gas emissions. Well-preserved fossil shells from the Campanian age (±78 Ma) high paleolatitude (50°N) coastal faunas of the Kristianstad Basin (southern Sweden) offer unique snapshot of short-term climate and environmental variability during the Campanian, which complement traditional long-term climate reconstructions. In this study, we apply a combination of high-resolution spatially resolved trace element analyses (µXRF and LA-ICP-MS), stable isotope analyses (IRMS) and growth modelling to study short-term (seasonal) variations recorded in the oyster species *Rastellum diluvianum* from Ivö Klack. A combination of trace element and stable isotope records of 12 specimens sheds light on the influence of specimen-specific and age-specific effects on the expression of seasonal variations in shell chemistry and allows disentangling vital effects from environmental influences in an effort to refine palaeoseasonality reconstructions of Late Cretaceous greenhouse climates. Growth modelling based on stable isotope records from *R. diluvianum* further allows to discuss the mode of life, circadian rhythm and reproductive cycle of extinct oysters and sheds light on their ecology. This multi-proxy study reveals that mean annual temperatures in the Campanian high-latitudes were 17 to 19°C with a maximum extent of seasonality of 14°C. These results show that the latitudinal gradient in mean annual temperatures during the Late Cretaceous was steeper than expected based on climate models and that the difference in seasonal temperature variability between latitudes was much smaller in the Campanian compared to today. Our results also demonstrate that species-specific differences and uncertainties in the composition of Late Cretaceous seawater prevent trace element proxies (Mg/Ca, Sr/Ca, Mg/Li and Sr/Li) to be used as reliable temperature proxies for fossil oyster shells.

1. Introduction

The Late Cretaceous was marked by a long cooling trend that brought global mean annual temperatures (MAT) down from the mid-Cretaceous climate maximum (±28°C surface ocean temperatures) in the Cenomanian and Turonian (±95 Ma) to slightly cooler temperatures (±22°C surface ocean temperatures) around the Campanian-Maastrichtian boundary (±72.1 Ma; Clarke and Jenkyns, 1999; Pearson et al., 2001; Huber et al., 2002; Friedrich et al., 2012; Scotese, 2016). This cooling trend was likely caused by a change in ocean circulation, initiated by the opening of the Equatorial Atlantic Gateway that separated the proto-North and -South Atlantic Ocean basins (Friedrich et al., 2009). It is well recorded in the white chalk successions of the Chalk Sea, which covered large portions of northwestern Europe during the Late Cretaceous Period (Reid, 1973; Jenkyns et al., 1994; Jarvis et al., 2002; Voigt et al., 2010). These chalk successions featured in various paleoclimate studies, because they are accessible in good outcrops and consist predominantly of calcareous nannofossils which faithfully record sea surface conditions (e.g. Jenkyns et al., 1994). Furthermore, the connection of the Chalk Sea to the (proto-)North Atlantic Ocean makes it an interesting area of study to constrain Late Cretaceous paleogeography and climate. Even with this prolonged cooling trend in the Late Cretaceous, proxy data and climate models show that the Campanian was still characterized by a relatively warm global climate with a shallow equatorial temperature gradient compared to today (Huber et al., 1995; Brady et al., 1998; Huber et al., 2002). Even though sea level changes seem to indicate possible small changes in land ice volume during the Late Cretaceous, warm high-latitude paleotemperatures seem to rule out the possibility of extensive polar ice sheets comparable in volume to modern ice caps (Barrera and Johnson, 1999; Huber et al., 2002; Jenkyns et al., 2004; Miller et al., 2005; Thibault et al., 2016). Given these climatic conditions and a relatively modern continental configuration, the Campanian serves as an interesting analogue for Earth's climate in the near future, should anthropogenic and natural emissions continue to contribute to the rise in global temperatures and decrease global ice volume on Earth (IPCC, 2013; Donnadieu et al., 2016). Most Late Cretaceous climate reconstructions focus on reconstructing and modelling long-term evolutions of humid/arid conditions on land and/or past atmospheric and oceanic temperatures (DeConto et al., 1999; Thibault et al., 2016; Yang et al., 2018). Data on the extent of seasonal variability from this time period, especially from high-latitudes, are scarce, although such data constitute a fundamental component of the climate system (Steuber, 1999; Steuber et al., 2005; Burgener et al., 2018).

https://doi.org/10.5194/bg-2019-74
Preprint. Discussion started: 25 September 2019

Fossil bivalve shells offer a valuable record for studying past climates on a seasonal scale. The chemistry of their shells records information on the environment in which bivalves grew, and incremental measurements of chemical changes along the growth direction (sclerochronological studies) potentially yield records of seasonal environmental changes (Mook, 1971; Jones, 1983; Klein et al., 1996a; Schöne and Gillikin, 2013). Their distribution allows paleoseasonality reconstructions across a wide range of latitudes (Roy et al., 2000; Jablonski et al., 2017), and the preservation potential of calcitic shell structures (especially in oyster shells) makes them ideal, if not one of the only, recorders of pre-Quarternary seasonality and sub-annual environmental change (Brand and Veizer, 1980; 1981; Al-Aasm and Veizer, 1986a; b; Immenhauser et al., 2005; Alberti et al., 2017). The incremental growth of bivalve shells in practice means that the limits in terms of time resolution of reconstructions from bivalve shells are governed by sampling resolution rather than the resolution of the record itself. While periods of growth cessation can occur (especially in high latitudes, Ullmann et al., 2010), in practice this allows reconstructions of changes down to sub-daily timescales given the right sampling techniques (Schöne et al., 2005; Sano et al., 2012; Warter et al., 2018; de Winter et al., in review). Examples of chemical proxies used for these paleoseasonality reconstructions include stable carbon and oxygen isotope ratios and trace element ratios (e.g. Steuber et al., 2005; Gillikin et al., 2006; McConnaughey and Gillikin, 2008; Schöne et al., 2011; de Winter et al., 2017a; 2018).

The incorporation of these chemical proxies into bivalve shells is challenged by the influence of so-called vital effects: biological controls on the incorporation of elements in the shell independent of the environment (Weiner and Dove, 2003; Gillikin et al., 2005). These vital effects have been shown to mask the characteristic relationships between shell chemistry and the environment, and appear to be distinct not only between different bivalve species but also between specimens of different ontogenetic age (Freitas et al., 2008). Differences between bivalve families mean that the chemistry of some taxa (like scallops: Family Pectinidae) are especially affected by vital effects (Lorrain et al., 2005; Freitas et al., 2008), while other families like oysters (Family Ostreidae) seem to be more robust recorders of environmental conditions (Surge et al., 2001; Surge and Lohmann, 2008; Ullmann et al., 2010; 2013). Nevertheless, the effect of changes in microstructure and the amount of organic matrix present in different parts of (oyster) shells on shell chemistry and preservation introduces uncertainty as to which parts of the shells are well-suited for reconstruction purposes (Carriker et al., 1991; Kawaguchi et al., 1993; Dalbeck et al., 2006; Schöne et al., 2010; 2013). The key to disentangling these vital effects from recorded environmental changes lies in the application of multiple proxies and techniques on the same bivalve shells (the “multi-proxy approach”; e.g. Ullmann et al., 2013; de Winter et al., 2017a; 2018) and to base reconstructions on more than one shell (Ivany, 2012).

The Kristianstad Basin is located on the southeastern Baltic Sea coast of the southern Swedish province of Skåne (56°2’ N, 14° 9’ E; see **Fig. 1**). Shallow marine sediments deposited at Ivö Klack consist of sandy and silty nearshore deposits containing carbonate gravel and are coarsely dated in the latest early Campanian (Christensen, 1975; 1984; Surlyk and Sørensen, 2010; Sørensen et al., 2015). The sediments were deposited in a near-shore setting described as a rocky coastline that was inundated during the maximum extent of the Late Cretaceous transgression, the paleolatitude is 50°N (Kominz et al., 2008; Csiki-Sava et al., 2015). Since the region has remained tectonically quiet since the Campanian, the deposits of Kristianstad Basin localities remain at roughly the same altitude as when they were deposited and have been subject to limited burial (Surlyk and Sørensen, 2010). The rocky shore deposits of Ivö Klack are characterized by a diverse shelly fauna, consisting of well-preserved fossils and fragments of brachiopods, belemnites, echinoids and asteroids, polychaete worms, gastropods, corals, ammonites and thick-shelled oysters, with a total of almost 200 different recognized species (Surlyk and Sørensen, 2010). In this diverse rocky shore ecosystem, various habitat zones can be distinguished, each with their distinct suite of organisms adapted to local conditions of varying amounts of sunlight, sedimentation and turbulence (Surlyk and Christensen, 1974; Sørensen et al., 2012). This unique combination of marine biodiversity and preservation of original shell material makes the localities in Kristianstad Basin ideal for studying sub-annual variability in shell chemistry and reconstructing paleoseasonality and environmental change in the Campanian (Sørensen et al., 2015).

In this study, we present a detailed, multi-proxy comparison of the growth and chemistry of well-preserved fossil shells of the thick-shelled oyster *Rastellum diluvianum* (Linnaeus, 1767) recovered from the Ivö Klack locality on the northern edge of the Kristianstad Basin. We combine stable isotope proxies conventional in

https://doi.org/10.5194/bg-2019-74
Preprint. Discussion started: 25 September 2019

sclerochronological studies ($\delta^{13}C$ and $\delta^{18}O$; e.g. Goodwin et al., 2001; Steuber et al., 2005) with less well-established trace element proxies (Mg/Ca, Sr/Ca, Mg/Li and Sr/Li; e.g. Bryan and Marchitto, 2008; Schöne et al., 2011; Füllenbach et al., 2015; Dellinger et al., 2018) and growth modelling based on $\delta^{18}O$ seasonality (Judd et al., 2018) in an attempt to disentangle the effects of growth rate, reproductive cycle and environmental change on shell chemistry. The data gathered in this study allow a detailed discussion on seasonal changes in temperature and water chemistry in the coastal waters of the Kristianstad Basin in the late early Campanian, as well as on the life cycle of *R. diluvianum* and its response to seasonal changes in its environment.

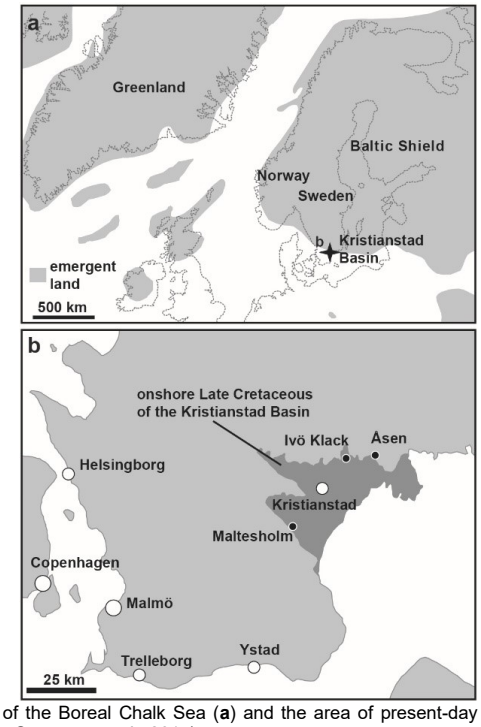

Figure 1: Paleogeographic map of the Boreal Chalk Sea (**a**) and the area of present-day southern Sweden (**b**) showing the location of Ivö klack (modified after Sørensen et al., 2015)

2. Materials and Methods

2.1 Sample acquisition and preparation

Complete valves of twelve individual *R. diluvianum* oysters were obtained from the Ivö Klack locality (see **Fig. 2**). Specimens of *R. diluvianum* were found *in situ* attached to the vertical sides of large boulders that characterized the rocky shore of Ivö Klack (Surlyk and Christensen, 1974). The valves were cleaned and fully embedded in Araldite® 2020 epoxy resin (Bodo Möller Chemie Benelux, Antwerp, Belgium). Dorsoventral slabs (±10 mm thick) were cut perpendicular to the hinge line using a water-cooled slow rotating saw with a diamond-coated blade (thickness ± 1 mm; **Fig. 2**). The surfaces cut on the central growth axis were progressively polished using silicon-carbide polishing disks (up to P2500, or 8.4 µm grain size). Polished surfaces were scanned at high (6400 dpi) resolution using an Epson Perfection 1650 flatbed color scanner (Seiko Epson Corp., Suwa, Japan). Resulting color scans of all polished *R. diluvianum* shell cross sections are provided in **Fig. 2** and **S1**. Shell microstructures in *R. diluvianum* shells were studied in detail on high-resolution scans and by using reflected light microscopy. Microstructural features were used to reconstruct the relative timing of shell growth (see **Fig. 3**). Fragments of visually well-preserved material from different microstructures in the shells were coated with gold and studied under a Scanning Electron Microscope (Quanta 200 ESEM) and imaged at 1000x – 2000x magnification (**Fig. 3b-e**). Chemical

https://doi.org/10.5194/bg-2019-74
Preprint. Discussion started: 25 September 2019

Biogeosciences
Discussions
Open Access
EGU

analyses were carried out on polished cross sections in order of sample size and destructive character of sampling (starting with the least destructive measurements).

Figure 2: Overview of the 12 *Rastellum diluvianum* shells used in this study. All shells are depicted on the same scale (see scalebar in center of image). Colors of the lines under sample names correspond to the colors of the lines in **Fig. 7** and **Fig. 9**. Every shell is represented by an image of the inside of the valve analyzed, as well as a color scan of the cross section through the shell on which high-resolution analyses were carried out. The dashed red line shows the location of these cross sections. The largest 5 shells (1-5, on top half) were sampled for IRMS analyses ($\delta^{13}C$ and $\delta^{18}O$). All shells were subjected to micro X-ray fluorescence (µXRF), laser ablation inductively coupled plasma mass spectrometry (LA-ICP-MS) and multi-cup inductively coupled plasma mass spectrometry (MC-ICP-MS) analyses. Full-size versions of the high-resolution color scans of shell cross sections are provided in **S1**.

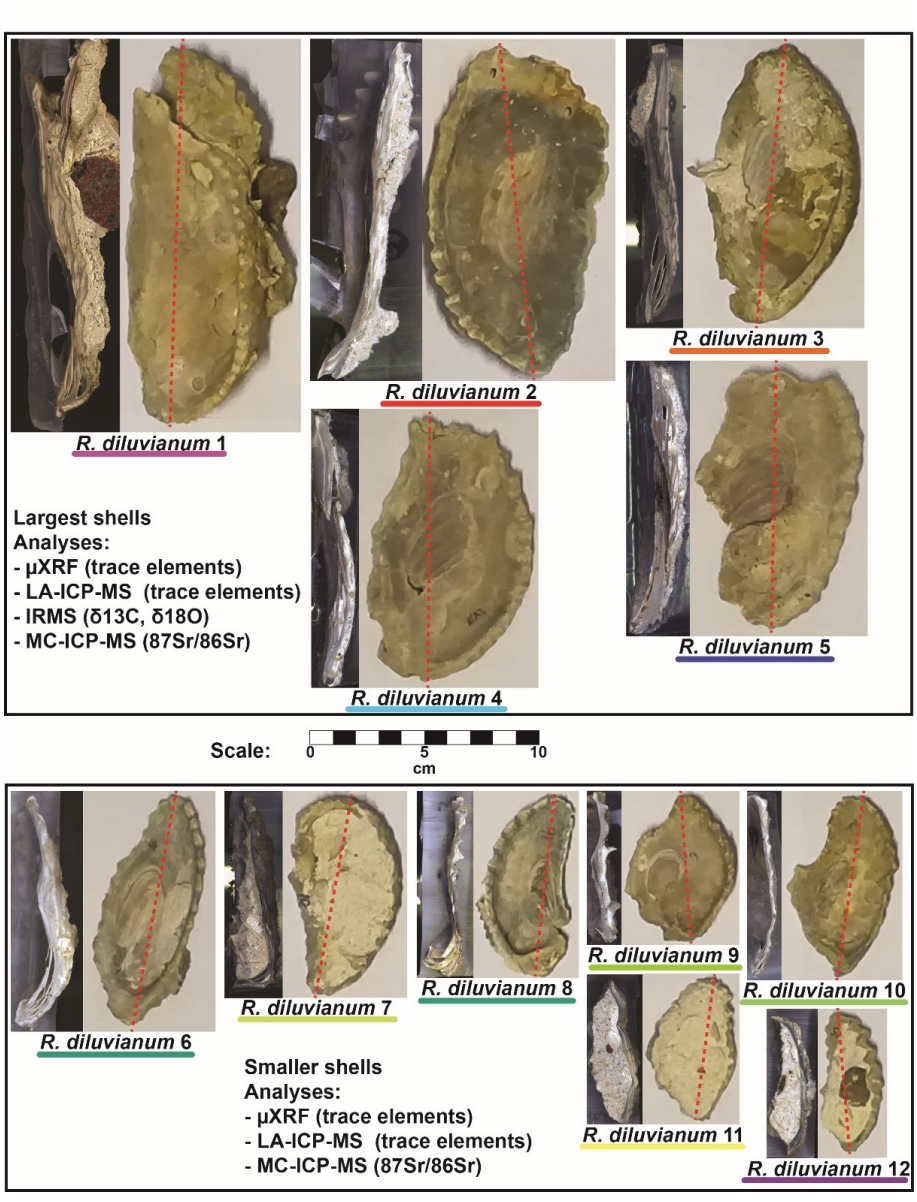

https://doi.org/10.5194/bg-2019-74
Preprint. Discussion started: 25 September 2019

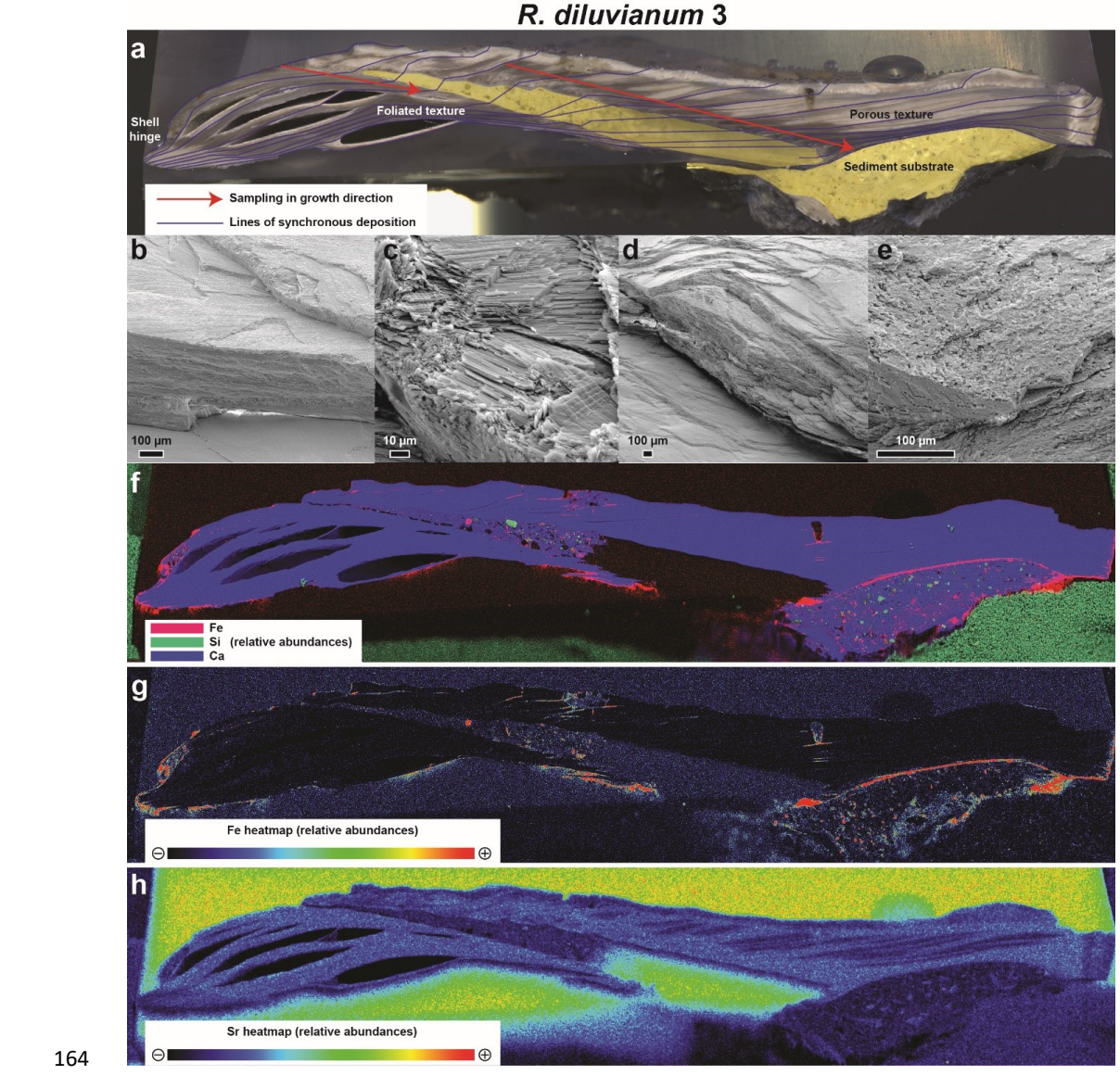

Figure 3: Overview image showing a high-resolution color scan of the cross section through *R. diluvianum* 3 (**a**) on which the different shell textures as well as the directions of high-resolution analyses (in growth direction) are indicated. Thin blue lines denote parts of the shell that were deposited at the same time (growth increments). (**b**) and (**c**) show SEM images of the well-preserved foliated calcite in the shell. More porous structures in the shell (vesicular calcite) are depicted in SEM images shown in (**d**) and (**e**). Below are shown three XRF elemental maps of the same cross section: A RGB-colored map displaying the relative abundances of Fe, Si and Ca (**f**), A heatmap of Fe concentrations (**g**; see scalebar below map) and a heatmap of Sr concentrations (**h**; see scalebar below map). XRF mapping only yields relative (semi-quantitative) abundance of elements.

2.2 Micro-XRF mapping

Elemental abundance maps of all *R. diluvianum* shell cross sections were obtained using a Bruker Tornado M4 energy-dispersive micro-X-Ray Fluorescence scanner (µXRF; Bruker nano GmbH, Berlin, Germany) All µXRF analyses carried out with the Bruker M4 Tornado are non-destructive. The µXRF is equipped with a Rh filament metal-ceramic tube X-Ray source operated at 50 kV and 600 µA (30 W; maximum energy

https://doi.org/10.5194/bg-2019-74
Preprint. Discussion started: 25 September 2019

settings). The circular spot projected on the same surface is estimated to have a diameter of 25 µm (Mo-Kα). A µm-precision XYZ translation stage allows for quick and precise sample movement such that a grid of 25 µm XRF spots can be measured on the sample surface by continuous scanning to construct elemental maps ($3 * 10^6$ - $5 * 10^6$ pixels per map). Exposure times of the X-ray beam per sampling position in mapping mode (1 ms/pixel) are too short to gain adequate signal-to-noise ratio for pixel-by-pixel quantification of elemental concentrations. Instead, processing of entire map surfaces using the Bruker Esprit™ software allows semi-quantitative elemental abundance maps to be created of the sample surface based on a mapping of the count rate in Regions of Interest of elements (see de Winter and Claeys, 2016; de Winter et al., 2017b; **Fig. 3**). XRF maps allow for a rapid assessment of the preservation state of original shell calcite based on variations in Si, Mn, Fe and Sr concentrations and guide the selection of sampling protocols for further analyses (de Winter and Claeys, 2016; **Fig. 3**). Results of XRF mapping on all 12 *R. diluvianum* shell cross sections are provided in **S2**.

2.3 Micro-XRF line scans

After XRF mapping, quantitative line scans were measured in growth direction on shell cross sections. Dwell times of 60 seconds per measurement yielded signal-to-noise ratios sufficient to allow individual points in line scans to be quantified. This acquisition time was chosen as to provide the optimal compromise between increasing run time (improved signal/noise ratio; enhanced reproducibility) and increasing the number of sampling positions (improving sampling density and allowing duplicate measurements) for the elements Mg, Al, Si, P, S, Ca, Ti, Mn, Fe, Cu, Zn and Sr (TSR and TSA; see discussion in de Winter et al., 2017b). The sampling density of line scans was 50 µm, adding up to a total of 11056 individual quantitative XRF spectra measured for this study. Spectra were quantified using the Bruker Esprit software calibrated using the matrix-matched BAS-CRM393 limestone standard (Bureau of Analyzed samples, Middlesbrough, UK), after which individual measurements were calibrated offline using 7 matrix-matched certified reference materials (CCH1, COQ1, CRM393, CRM512, CRM513, ECRM782 and SRM1d), which were treated as samples (see Vansteenberge et al., in review). R^2 values of calibration curves exceeded 0.99 and reproducibility standard deviations were better than 10% relative to the mean. Even though line scans were positioned on well-preserved shell calcite based on the XRF map results, a second check was carried out in which individual points were rejected based on conservative thresholds for diagenetic recrystallization or detrital contamination ([Ca] < 38 wt%, [Si] > 1 wt%, [Mn] > 200 µg/g or [Fe] > 250 µg/g; [Sr]/[Mn] < 100 mol/mol; see Al-Aasm and Veizer, 1986a; Sørensen et al., 2015). Concentrations of Ca, Mg and Sr in well-preserved shell sections were used to explore the potential of Mg/Ca and Sr/Ca molar ratios as paleoenvironmental proxies. Unprocessed results of XRF line scanning are provided in **S3**.

2.4 LA-ICP-MS line scans

Spatially resolved elemental concentrations for Li, B, Mg, Si, P, Ca, Ti, V, Cr, Mn, Fe, Ni, Zn, Rb, Sr, Ba, Pb and U were calculated from a calibrated transient MS signal recorded during line scanning in the growth direction (parallel to the XRF line scans) on the shell cross sections using Laser Ablation-Inductively Coupled Plasma-Mass Spectrometry (LA-ICP-MS). LA-ICP-MS measurements were carried out at the Atomic and Mass Spectrometry – A&MS research unit of Ghent University (Ghent, Belgium) using a 193 nm ArF*excimer-based Analyte G2 laser ablation system (Teledyne Photon Machines, Bozeman, USA), equipped with a HelEx 2 double-volume ablation cell, coupled to an Agilent 7900 quadrupole-based ICP-MS unit (Agilent, Tokyo, Japan). Continuous scanning along shell transects using a laser spot with a diameter of 25 µm, scan speed of 50 µm/s and detector mass sweep time of 0.5 yielded profiles with a lateral sampling interval of 25 µm, amounting to a total of 9505 LA-ICP-MS data points gathered. The aerosol was transported using He carrier gas into the ICP-MS unit via the aerosol rapid introduction system (ARIS; Teledyne Photon Machines, Bozeman, USA). Elemental concentrations were calibrated using bracketed analysis runs on US Geological Survey (USGS) BCR-2G, BHVO-2G, BIR-1G, GSD-1G and GSE-1G and National Institute of Standards and Technology (NIST) SRM612 and SRM610 certified reference materials. Calcium concentrations (measured via ^{43}Ca) were used as internal standard for data normalization and drift correction during the measurement campaign, and Ca concentrations of 38.5 wt% were assumed for pristine shell carbonate. Coefficients of determination (R^2) of a linear model fitted to the calibration curves were better than 0.99 and the standard deviation of reproducibility for elemental concentrations was better than 5% relative to the mean value. Individual LA-ICP-MS measurements were inspected for diagenetic alteration or contamination by detrital material using the same thresholds as used for XRF data (see above). LA-ICP-MS and µXRF measurements were combined to cover a wider range of

https://doi.org/10.5194/bg-2019-74
Preprint. Discussion started: 25 September 2019

231 elements, since some elements (e.g. S and Sr) were measured more reliably using µXRF, while others
232 (e.g. Li or Ba) could only be determined using LA-ICP-MS. Concentrations of Li, Mg, and Sr were used to
233 explore the potential of Mg/Li and Sr/Li molar ratios as proxies for paleoenvironmental change.
234 Unprocessed results of LA-ICP-MS line scans are provided in **S4**.

235 2.5 Isotope Ratio Mass Spectrometry

236 A transect of powdered samples (±200 µg) was sampled for Isotope Ratio Mass Spectrometry (IRMS)
237 analysis in growth direction along well-preserved foliated calcite (**Fig. 3**) in the five largest of the twelve *R.*
238 *diluvianum* shells (*R. diluvianum* 1-5; see **Fig. 2**) using a microdrill (Merchantek/Electro Scientific Industries
239 Inc., Portland (OR), USA) equipped with a 300 µm diameter tungsten carbide drill bit, coupled to a
240 microscope (Leica GZ6, Leica Microsystems GmbH, Wetzlar, Germany). A total of 531 IRMS samples were
241 taken at an interspacing of 250 µm. Stable carbon and oxygen isotope ratios ($\delta^{13}C$ and $\delta^{18}O$) were
242 measured in a NuPerspective IRMS equipped with a NuCarb carbonate preparation device (Nu
243 Instruments, UK). The sample size (50-100 µg) allowed duplicate measurements to be carried out regularly
244 to assess reproducibility. Samples were digested in 104% phosphoric acid at a constant temperature of
245 70°C and the resulting CO_2 gas was cryogenically purified before being led into the IRMS through a dual
246 inlet system. Isotope ratios were corrected for instrumental drift and fractionation due to variations in sample
247 size and the resulting values are reported in per mille ratios calibrated to the Vienna Pee Dee Belemnite
248 standard (‰VPDB) using repeated measurements of the IA-603 stable isotope standard (International
249 Atomic Energy Agency, Vienna, Austria). Reproducibility of $\delta^{18}O$ and $\delta^{13}C$ measurements on this standard
250 were better than 0.1‰ and 0.05‰ (1σ; N=125) respectively. All stable isotope analysis results are provided
251 in **S5** and plots of stable isotope and trace element records from all shells are shown in **S6**.

252 2.6 Growth and age modelling

253 Stable oxygen isotope curves measured in *R. diluvianum* were used to produce age models for the growth
254 of the shell using a bivalve growth model written in MatLab (Mathworks, Natick, MA, USA) which simulates
255 $\delta^{18}O$ curves using a combination of a growth sinusoid and a temperature sinusoid to fit the $\delta^{18}O$ data (Judd
256 et al., 2018). This simulation model was modified to calculate its temperatures based on calcite $\delta^{18}O$
257 (following Kim and O'Neil, 1997) rather than from the aragonite $\delta^{18}O$-temperature relationship used in the
258 original approach (after Grossman and Ku, 1986; see Judd et al., 2018). A value of -1.0‰ VSMOW was
259 assumed for $\delta^{18}O$ of Campanian ocean water (Thibault et al., 2016). Additional minor modifications in the
260 source code allowed results of intermediate calculation steps in the model to be exported. The modified
261 Matlab source code is provided in **S7**. Note that this model assumes that the shape and absolute value of
262 $\delta^{18}O$ curves depend solely on water temperature and growth rate (ignoring changes in sea water $\delta^{18}O$), and
263 that a modelled year contains 365 days by construction (while this number should be slightly larger in the
264 Late Cretaceous; e.g. Meyers and Malinverno, 2018; de Winter et al., in review). Nevertheless, shell
265 chronologies reconstructed from seasonal patterns in $\delta^{18}O$ should still be reliable regardless of their origin.
266 Uncertainties on modelled temperature curves were derived by propagating the measurement uncertainty
267 on $\delta^{18}O$. Age models thus obtained for shells *R. diluvianum* 1-5 were used to align all proxy records on a
268 common time axis. Age models for *R.diluvianum* 6-12 were constructed by extrapolating relationships
269 between modelled seasonality and microstructures and trace element concentrations observed in *R.*
270 *diluvianum* 1-5. Simultaneously deposited microstructural features in shell cross sections (see **Fig. 3**) were
271 used to determine the actual dorsoventral height of the shells at different ages, linking shell height to the
272 age and allowing the construction of growth curves for all twelve *R. diluvianum* shells.

273 2.7 Strontium isotopic analysis

274 Samples (26 mg) for strontium isotopic analysis were obtained by drilling the well-preserved foliated calcite
275 in all shells using a Dremel 3000 dental drill with a 0.5 mm tungsten carbide drill bit. Calcite samples were
276 dissolved in subboiled concentrated (14 M) nitric acid (HNO_3) at 120°C and left to dry out at 90°C overnight,
277 after which the residue was redissolved in 1 M HNO_3. Strontium in the samples was purified following the
278 ion-exchange resin chromatography method detailed in Snoeck et al. (2015). The $^{87}Sr/^{86}Sr$ of purified Sr
279 samples were determined using a Nu Plasma (Nu Instruments Ltd, Wrexham, UK) multi-collector (MC) ICP-
280 MS unit in operation at the Université Libre de Bruxelles (ULB). During the measurement run, repeated
281 analyses of NIST SRM987 standard solution yielded a ratio of 0.710250 ± 40 (2 SD; N = 14), statistically
282 consistent with the literature value of 0.710248 ± 5.8 (2 s.e.; McArthur et al., 2001; Weis et al., 2006). All

https://doi.org/10.5194/bg-2019-74
Preprint. Discussion started: 25 September 2019

283 results were corrected for instrumental mass discrimination by internal normalization and normalized to the
284 literature value of NIST SRM987 (0.710248) through a standard-sample bracketing method. For each
285 sample, $^{87}Sr/^{86}Sr$ are reported with a 2 standard deviations uncertainty (**S8**).

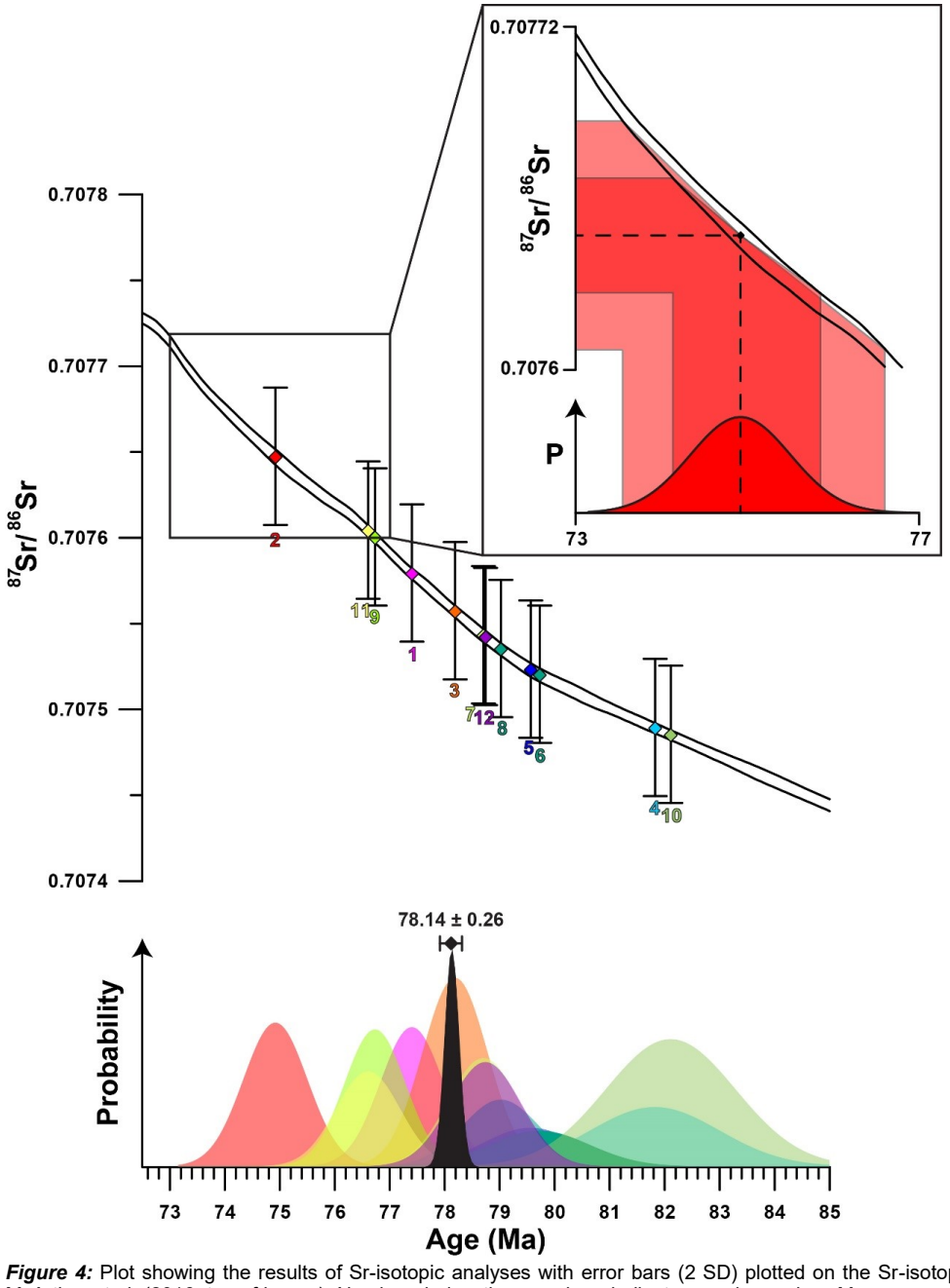

286 ***Figure 4:*** Plot showing the results of Sr-isotopic analyses with error bars (2 SD) plotted on the Sr-isotope curve of
287 McArthur et al. (2016; top of image). Numbers below the error bars indicate sample number. Measurements from the
288 12 specimens of *R. diluvianum* are represented by parallelograms in different shades of blue which correspond to the
289 graph below. The probability distribution curves in the lower pane show the distribution of uncertainty on each Sr-

https://doi.org/10.5194/bg-2019-74
Preprint. Discussion started: 25 September 2019

isotope measurement as well as the uncertainty on the Sr-isotope curve propagated to the age domain (colors of individual shells are the same as in **Fig. 2**). Insert shows schematically how uncertainties of the isotope measurements as well as the isotope curve are propagated into the age domain. The black curve shows the total uncertainty distribution function compiled from the 12 individual measurements following Barlow (2004), with the combined age estimate including uncertainty (2 SD) shown above.

2.8 Strontium isotope dating

R. diluvianum specimens were independently dated by comparing $^{87}Sr/^{86}Sr$ values measured in the samples with the Sr-isotope curve in the 2016 Geological Timescale (McArthur et al., 2016). Uncertainties in $^{87}Sr/^{86}Sr$ measurements were propagated into dates by finding the closest date of the mean $^{87}Sr/^{86}Sr$ value as well as the dates of the minimum (-2σ) and maximum (+2σ) $^{87}Sr/^{86}Sr$ values by linearly interpolating ages in the $^{87}Sr/^{86}Sr$ curve matching the measured $^{87}Sr/^{86}Sr$ value, including the uncertainty estimated on the Sr-isotope curve itself. A composite age for the Ivö Klack deposits was obtained by combining the age uncertainty distributions of the individually dated $^{87}Sr/^{86}Sr$ samples into a single age. Due to the non-linear shape of the $^{87}Sr/^{86}Sr$ curve, uncertainties on the $^{87}Sr/^{86}Sr$ ages were asymmetrical. Since no mathematical solution exists for the combination of asymmetric uncertainties, the asymmetric uncertainty on the total age has to be approximated through maximum likelihood estimation using the combined log likelihood function (Barlow, 2003). The approximation of the total uncertainty of combined $^{87}Sr/^{86}Sr$ dating results in this study was carried out using the mathematical approach of Barlow (2004) in R (R Core Team, 2013; Roger Barlow, personal communication; code available on https://zenodo.org/record/1494909). The uncertainty interval of the composite age is represented by 2 times the standard error (~95.5% confidence level). A plot of the uncertainty distributions of the individual specimens and the total uncertainty distribution is shown in **Fig. 4**. Raw $^{87}Sr/^{86}Sr$ data is provided in **S8**.

3. Results

3.1 Dating

The compilation of $^{87}Sr/^{86}Sr$ results from 12 specimens of *R. diluvianum* (**Fig. 4**) shows how age estimates from individual specimens have considerable uncertainties (standard deviations around 1 Myr, see **S8**), yet the uncertainty on the composite age is significantly smaller. The composite age for the Ivö Klack deposits is 78.14 Ma (±0.26; 2 standard errors). This result places the age of the Ivö Klack deposits close to the early/late Campanian boundary when applying a twofold division of the Campanian and in the middle Campanian when applying a threefold division scheme (Ogg et al., 2016). This age estimate is similar to the age obtained when plotting the *B. mammilatus* zone on the recent integration schemes of the Campanian (Wendler, 2013). Earlier estimates (Christensen, 1997; Surlyk and Sørensen, 2010; Sørensen et al., 2015) yielded ages about 2-4 Myr older (80-82 Ma), but those relied on presently outdated and partly incorrect age models.

3.2 Shell structure and preservation

A combination of high-resolution color scans, SEM images and µXRF mapping of shell cross sections reveals that *R. diluvianum* shells consist of thin layers of dark, foliated calcite, interwoven with lighter, more porous carbonate layers. The latter are characterized by higher concentrations of Mn, Fe and Si and lower Sr concentrations (**Fig. 3**). Foliated calcite layers are more densely packed on the inside of the shell, especially in the region of the adductor muscle scar (**Fig. 3**). They are characterized by high Sr concentrations and low concentrations of Mn, Fe and Si (**Fig. 3**; **S2**). Foliated layers are also densely packed at the shell hinge. Further away from the shell hinge and the inside of the valve, porous carbonate layers become more dominant. In these regions, µXRF mapping also clearly shows that detrital material (high in Si and Fe) is often found between the shell layers. SEM images show that the shell structure of *R. diluvianum* strongly resembles to that of modern oyster species, as described in previous studies (Carriker et al., 1979; Surge et al., 2001; Ullmann et al., 2010; 2013; Zimmt et al., 2018). The major part of the shell consists of (foliated and porous) calcite structures, which were sampled for chemical analyses in this study. As in modern oyster species, aragonite may originally have been deposited on the resilium of the shell, but this region is not considered for analyses (Stenzel, 1963; Carriker et al., 1979; Sørensen et al., 2012). Close

https://doi.org/10.5194/bg-2019-74
Preprint. Discussion started: 25 September 2019

similarities with modern oysters allow to infer that shell growth in *R. diluvianum* occurred in a similar way as it does in modern oyster species like *Ostrea edulis*, *Crassostrea virginica* and *C. gigas*. This extrapolation allows to estimate the total shell height from microstructural growth markers (**Fig. 3**; following Zimmt et al., 2018), linking growth to changes in shell chemistry. It also allows chemical changes in the shell to be interpreted in terms of environmental changes by applying calibration curves for trace element proxies that were previously established for modern oyster species (e.g. Surge and Lohmann, 2008; Ullmann et al., 2013; Mouchi et al., 2013; Dellinger et al., 2018).

3.3 Trace element analyses results

The combination of µXRF, LA-ICP-MS and IRMS analyses on *R. diluvianum* shells resulted in multi-proxy records of changes in Mg/Ca, Sr/Ca (µXRF), Mg/Li, Sr/Li (LA-ICP-MS), $\delta^{13}C$ and $\delta^{18}O$ (IRMS, only for shells 1-5, see **Fig. 2**). All chemical analyses were carried out on the dense foliated calcite exposed in cross sections close to the inner edge of the shell valve (**Fig. 3**). High-resolution color scans and detailed recording of sampling positions allowed these records to be plotted on a common axis (see **S6**). In **Fig. 5**, results of chemical analyses of *R. diluvianum* specimens (including diagenetic parts) are compared with data from three other mollusk taxa (*Belemnellocamax mammillatus*, *Acutostrea incurva* and radiolithid rudists) from Ivö Klack (Sørensen et al., 2015), as well as data from extant oysters (Rucker and Valentine, 1961; Surge et al., 2001; Ullmann et al., 2013). **Figure 5** shows that stable isotope ratios of the rudist and oyster shells overlap, while belemnites are characterized by much lower $\delta^{13}C$ and heavier $\delta^{18}O$ values. This suggests that $\delta^{13}C$ in belemnite rostra are affected by vital effects while heavier $\delta^{18}O$ values of the belemnites suggest that these animals lived most of their life span in a different environment than the bivalves (deeper waters), as previously suggested by Sørensen et al. (2015). By contrast, stable isotope ratios recorded in the bivalve shells overlap and match the isotope ratios measured in Campanian chalk deposited in the neighboring Danish Basin (Thibault et al., 2016). Multi-proxy analysis revealed periodic variations in stable isotope and trace element ratios (see **Fig. 6**). The amplitudes of these variations plotted in **Fig. 5** show that Mg and Sr concentrations measured in all three fossil bivalve taxa are similar, while concentrations in the belemnite rostra are much higher. Finally, plots of Sr and $\delta^{18}O$ against Mn concentrations demonstrate that diagenetic alteration (evident from elevated Mn concentrations) reduces the Sr concentration in carbonate of all four taxa. Stable oxygen isotope ratios of the shells are affected to a lesser degree. The vast majority of measurements in all four taxa show very little signs of diagenetic alteration, with most measurements characterized by low (< 100 µg/g) Mn concentrations (**Fig. 5**).

https://doi.org/10.5194/bg-2019-74
Preprint. Discussion started: 25 September 2019

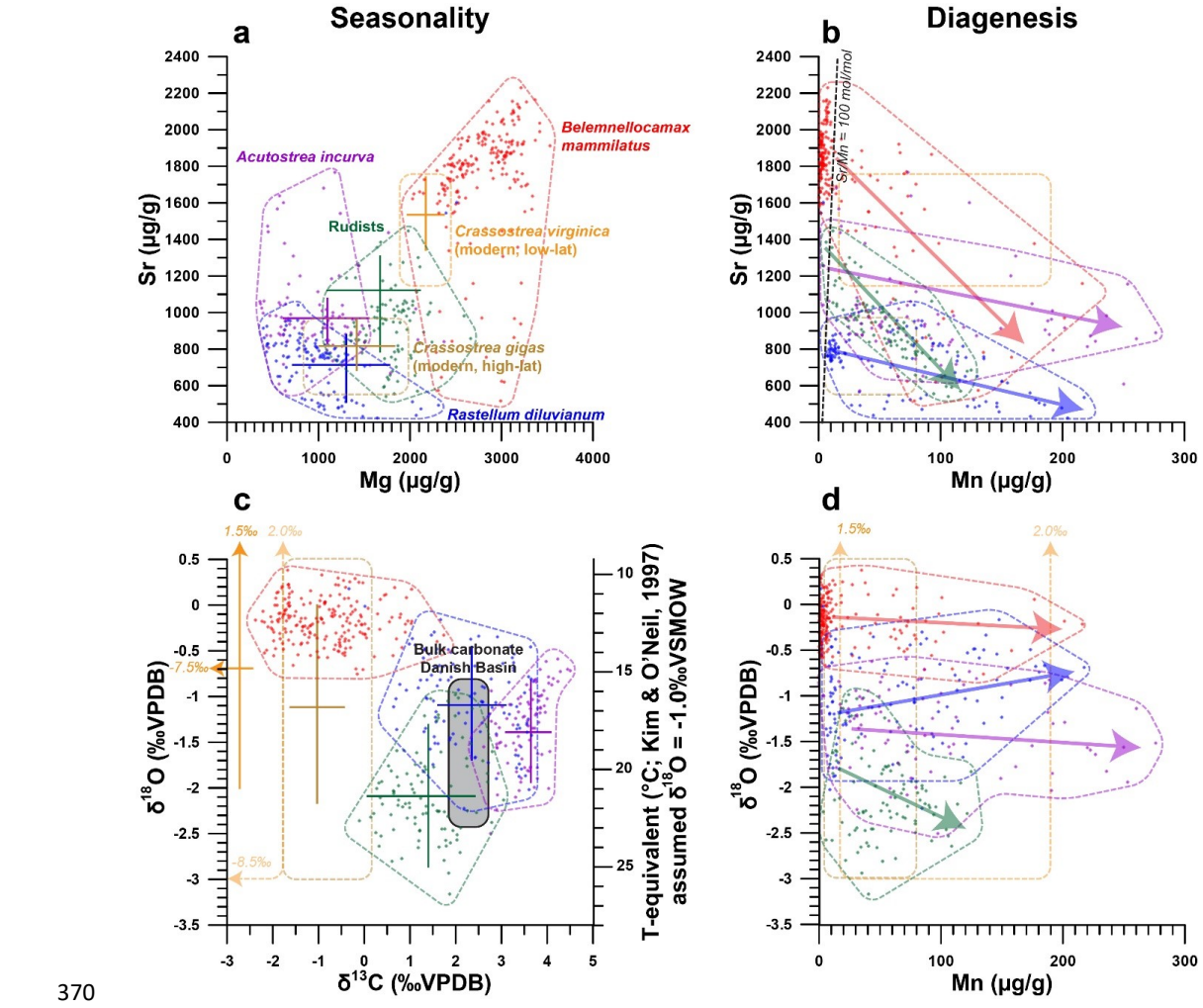

Figure 5: Cross plots summarizing the results of trace element and stable isotope analyses of the oysters *R. diluvianum* (blue), *A. incurve* (purple), associated rudist bivalves (green) and the belemnite *B. mammilatus* (red, after Sørensen et al., 2015) from the Kristianstad basin. Results in modern *C. gigas* (grey/black; Ullmann et al., 2013) and *C. virginica* (orange/yellow; Rucker and Valentine, 1961; Surge et al., 2001) oysters are plotted for comparison. Points indicate individual data points, drawn polygons illustrate the range of the data and crosses indicate the extent of seasonality (if present). (**a**) Strontium concentrations plotted against magnesium concentrations. (**b**) Strontium concentrations plotted against manganese concentrations. Arrows indicate the interpreted direction of diagenetic alteration and the black dashed line shows the Sr/Mn diagenesis threshold proposed by Sørensen et al. (2015; 100 mol/mol). (**c**) $\delta^{18}O$ plotted against $\delta^{13}C$. Grey area indicates the range of stable isotope ratios measured in Campanian chalk deposits from the nearby Danish Basin by Thibault et al. (2016) (**d**) $\delta^{18}O$ plotted against manganese concentrations, with arrows indicating proposed direction of diagenetic alteration.

3.4 Stable isotope records

Records of $\delta^{13}C$ and $\delta^{18}O$ in the growth direction through *R. diluvianum* shells exhibit periodic variations. These variations are much more regular in $\delta^{18}O$ records, which show extreme values of -3‰ up to 0‰ VPDB. Some shells, such as *R. diluvianum* 3 (**Fig. 6**), exhibit longer term trends on which these periodic variations are superimposed. These trends suggest the presence of multi-annual cyclicity with a period in the order of 10-20 years, but the length of *R. diluvianum* records (max. 10 years) is smaller than the estimated period of these changes and is therefore not sufficient to statistically validate the presence of this

https://doi.org/10.5194/bg-2019-74
Preprint. Discussion started: 25 September 2019

cyclicity. The extreme values in $\delta^{18}O$ records translate to temperatures in the range of extremes of 12°C to 26°C when assuming a constant $\delta^{18}O_{seawater}$ value of -1.0‰ (e.g. Thibault et al., 2016) and applying the temperature relationship of Kim and O'Neil (1997). Carbon isotope ratios ($\delta^{13}C$) do not always follow the same trends as $\delta^{18}O$ records. In many parts of *R. diluvianum* shells, there is a clear covariation between the two isotope ratios, suggesting $\delta^{13}C$ is affected by seasonal changes. However, in other parts this correlation is less clear, suggesting that other (non-seasonal) factors play a role in determining the $\delta^{13}C$ of shell material. Superimposed on these changes, a statistically significant ontogenetic trend can be discerned in the $\delta^{13}C$ records of 10 out of 12 shells. However, the scale and direction of these trends do not seem consistent between shells.

3.5 Age models

Modelling the growth of *R. diluvianum* bivalves from seasonal variations in $\delta^{18}O$ profiles yielded age models, growth rate estimates and reconstructions of water temperature variations during the lifetime of the bivalves. Due to the clear seasonal patterns in $\delta^{18}O$ records (**Fig. 6**), modelled $\delta^{18}O$ profiles closely approximated the measured $\delta^{18}O$ profiles (total $R^2 = 0.86$, N = 412, see **S9**), lending high confidence to shell age models. Modelling allowed all proxies measured in the shells of *R. diluvianum* to be plotted against shell age, clearly revealing the influence of seasonal variations in environmental parameters on shell chemistry (**S10**). When plotting all proxies on the same time axis, clear ontogenetic trends emerge in Mg/Li, Sr/Li and $\delta^{13}C$ in nearly all specimens of *R. diluvianum*. Trends and variations in Mg/Li and Sr/Li are strongly correlated, suggesting that variation in both these trace element ratios is largely driven by variations in Li concentrations. Linear regression was applied to isolate ontogenetic trends in $\delta^{13}C$ and Li/Ca ratios (**S11-S12**). While most of these ontogenetic trends are statistically significant ($p < 0.05$), they are highly variable between specimens, both in terms of direction and magnitude. The distribution of slopes of ontogenetic trends in Li/Ca and $\delta^{13}C$ cannot be distinguished from random variation (see **Table 1**). Therefore, no predictable ontogenetic trends were found for $\delta^{13}C$ and Li-proxies in *R. diluvianum* shells.

	Li/Ca			$\delta^{13}C$		
	slope (mol/(mol*yr))	R2	p-value	slope (‰/yr)	R2	p-value
***R. diluvianum* 1**	-1.29E-06	0.053	4.32E-08	0.346	0.426	8.86E-07
***R. diluvianum* 2**	3.74E-07	0.101	2.68E-05	0.169	0.440	8.19E-08
***R. diluvianum* 3**	3.86E-07	0.004	5.32E-03	-0.004	0.001	8.09E-01
***R. diluvianum* 4**	-1.07E-06	0.025	8.78E-04	0.023	0.009	3.99E-01
***R. diluvianum* 5**	-1.94E-06	0.030	6.30E-14	0.136	0.492	5.53E-11
***R. diluvianum* 6**	-2.32E-06	0.117	8.75E-15			
***R. diluvianum* 7**	-7.49E-07	0.029	4.77E-02			
***R. diluvianum* 8**	-1.19E-07	0.003	2.90E-01			
***R. diluvianum* 9**	-4.63E-07	0.010	5.65E-02			
***R. diluvianum* 10**	1.59E-06	0.015	1.61E-02			
***R. diluvianum* 11**	-1.87E-06	0.199	4.25E-12			
***R. diluvianum* 12**	-4.55E-07	0.003	4.19E-01			
$p(\chi^2)$			0.976	$p(\chi^2)$		1.000
$p(\chi^2)$ weighed by R2			0.976	$p(\chi^2)$ weighed by R2		1.000
$p(\chi^2)$ weighed by p-value			0.961	$p(\chi^2)$ weighed by p-value		0.998

Table 1: *Overview of the slopes of ontogenetic trends in Li/Ca and $\delta^{13}C$ records. P-values on the bottom of the table show that the distribution of slopes is statistically indistinguishable from random.*

https://doi.org/10.5194/bg-2019-74
Preprint. Discussion started: 25 September 2019

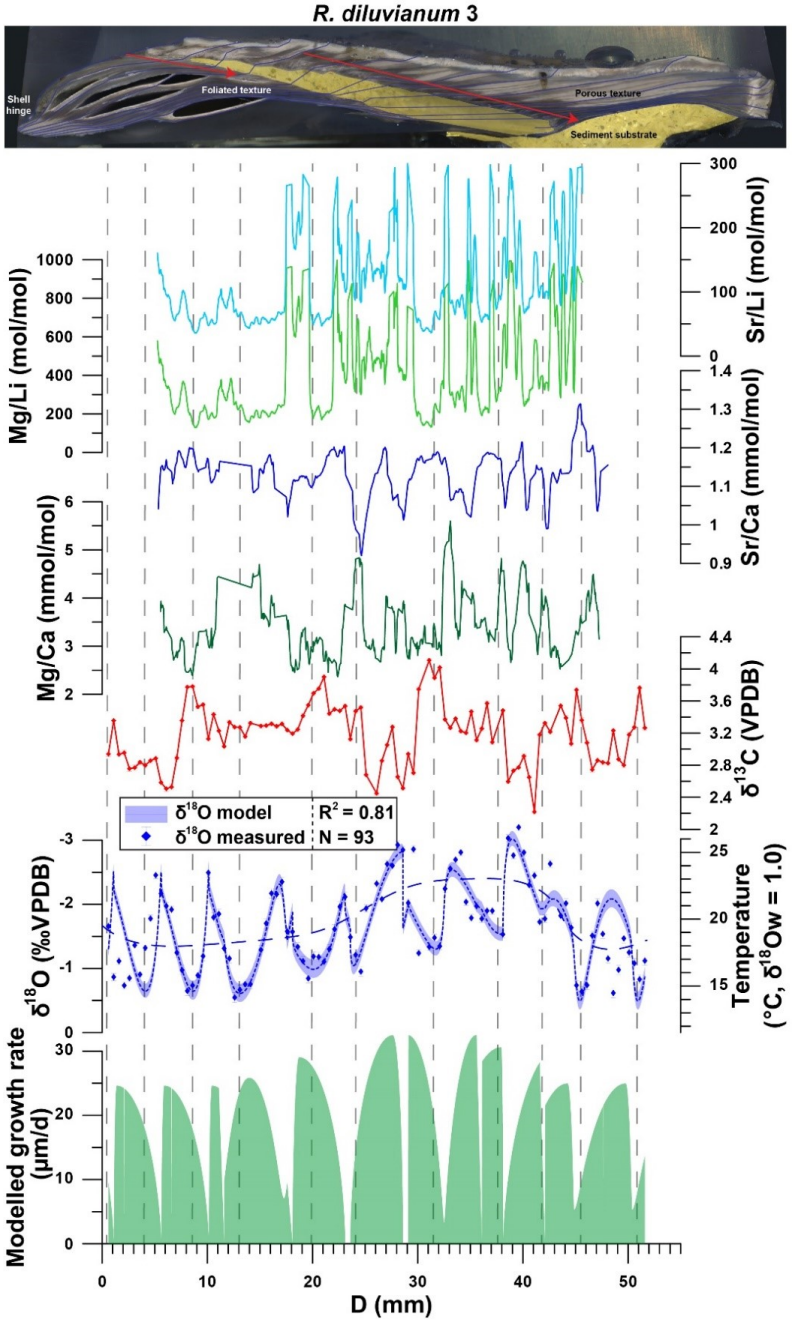

Figure 6: Example of multi-proxy records measured in *R. diluvianum* specimen 3 plotted against distance in growth direction (see image on top and **Fig. 3** for reference). From top to bottom, records of Sr/Li (light blue), Mg/Li (light green), Sr/Ca (dark blue), Mg/Ca (dark green), $\delta^{13}C$ (red), $\delta^{18}O$ (blue dots with error bars) and modelled growth rate (light green fill) are plotted. The shaded blue curve plotted underneath the $\delta^{18}O$ record illustrates the result of growth and $\delta^{18}O$ modelling and its propagated error (vertical thickness of curve, 2SD). The dashed blue curve plotted on top of the $\delta^{18}O$ record shows the observed multi-annual trend in the data.

415

https://doi.org/10.5194/bg-2019-74
Preprint. Discussion started: 25 September 2019

3.6 Trace element seasonality

A comparison of the amplitude of periodic variations in Mg/Ca, Sr/Ca, Mg/Li and Sr/Li in 12 *R. diluvianum* shells (**Fig. 7**), together with a tentative interpretation in terms of temperature seasonality, reveals that it is not straightforward to apply the transfer functions previously proposed for these proxies on fossil bivalve shells. Results reveal a strong positive inter-shell correlation between Sr/Li and Mg/Ca (R^2 = 0.76) and between Sr/Li and Mg/Li (R^2 = 0.93), while positive correlations between Sr/Ca and Mg/Ca (R^2 = 0.19) as well as between Sr/Ca and Mg/Li (R^2 = 0.20) are weak. The Mg/Li temperature regressions based on benthic foraminifera (Bryan and Marchitto, 2008) yield unrealistically high-water temperatures (> 50°C), presumably due to typically lower Mg concentrations in foraminifera compared to bivalves (Yoshimura et al., 2011). The Mg/Ca and Sr/Li temperature relationships (Surge and Lohmann, 2008; *C.* virginica; and Füllenbach et al., 2015; *Cerastoderma edule*; respectively) and a Mg/Li temperature regression based on the calcitic bivalve *Mytilus edulis* (Dellinger et al., 2018) yield temperatures in the same range as those reconstructed from local bulk carbonate stable isotope measurements (10-20°C; e.g. Thibault et al., 2016), but Sr/Li-based temperatures display a pattern opposite to those based on Mg-proxies. This seems to suggest that, if trace element concentrations in *R. diluvianum* are linked to temperature, the temperature relationship of Mg-based proxies and the Sr/Li proxy are discordant and cannot both be applicable to *R. diluvianum*. These results raise difficulties similar to those that arose in earlier attempts to apply trace element ratios for water temperature reconstructions in fossil mollusks (Steuber, 1999; Weiner and Dove, 2003; de Winter et al., 2017a). The interpretation of these records is further complicated by large intra-specific variability in the incorporation of Mg into biogenic carbonates (e.g. Schöne et al., 2010) and the lack of constraints of seawater compositions in the Late Cretaceous (e.g. Stanley and Hardie, 1998; especially with respect to Li concentrations). It shows that trace element ratios in these shells can only be interpreted with some degree of confidence when combined with stable isotope records from shells of the same setting and species.

https://doi.org/10.5194/bg-2019-74
Preprint. Discussion started: 25 September 2019

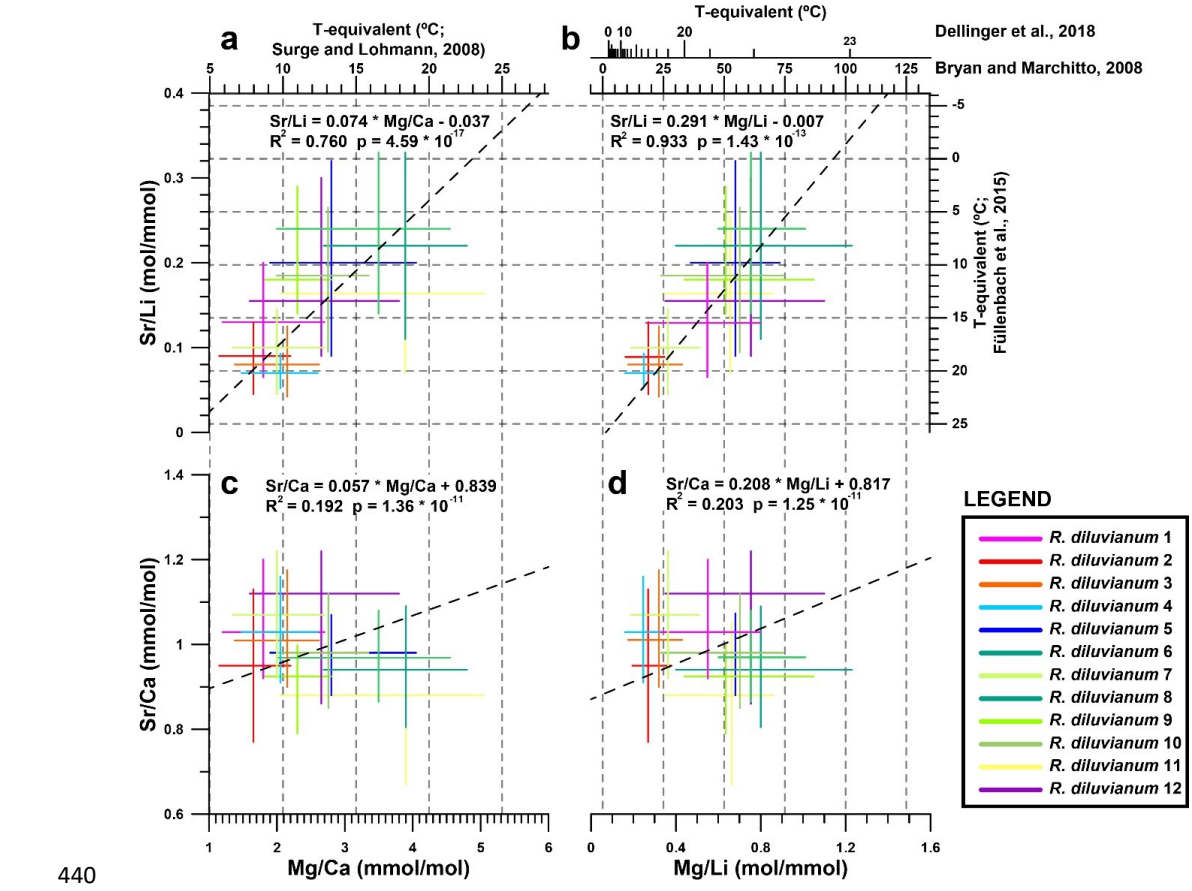

Figure 7: Cross plots showing the extent of interpreted seasonality observed in records of four trace element proxies in all 12 *R. diluvianum* specimens. Colors of lines of individual shells correspond to colors indicated in **Fig. 2**. Temperature conversions from previously published regressions of the proxies with temperature are shown on opposite axes with grey dashed lines corresponding to major tick marks on the temperature scale (**a**) Sr/Li plotted against Mg/Ca showing a strong significant intra-shell correlation. (**b**) Sr/Li plotted against Mg/Li showing a strong significant intra-shell correlation due to dominant variations in Li concentration. Note that two different Mg/Li temperature calibrations were explored. (**c**) Sr/Ca plotted against Mg/Ca showing weak but significant intra-shell correlation. (**d**) Sr/Ca plotted against Mg/Li showing a weakly significant intra-shell correlation. Data for this plot is found in **S13**.

3.7 Temperature seasonality

The seasonal variation in all specimens of *R. diluvianum* was aligned and stacked relative to shell age models (**Fig. 8**). This composite stack shows that the seasonal temperature range in Ivö Klack during the late early Campanian was between 16°C and 21°C when assuming constant seawater $\delta^{18}O$. Modelled growth rates in *R. diluvianum* peak near the end of the low temperature season and average growth rates are lowest shortly after the temperature maximum (**Fig. 8**). This phase shift between temperature and growth rate could indicate that growth in *R. diluvianum* in this setting was not limited by low temperatures, as observed in modern mid- to high-latitude oysters (Lartaud et al., 2010). High temperature extremes (>25°C) may have slowed or stopped growth, as recorded in modern low latitude settings (Surge et al., 2001), but $\delta^{18}O$-seasonality suggests that these temperatures were not common at the Ivö Klack locality. Mg/Ca ratios in *R. diluvianum* exhibit a clear seasonal pattern, which is inversely correlated with temperature, while Mg/Ca ratios in foliate calcite of modern oysters show opposite correlation with temperature (Surge and Lohmann, 2008; Mouchi et al., 2013) or exhibit no correlation at all (Ullmann et al., 2013). Sr/Ca ratios in *R. diluvianum* are positively correlated with seasonal temperature variations. Mg/Li and Sr/Li ratios show no correlation with temperature. Instead, both proxies display elevated values both

https://doi.org/10.5194/bg-2019-74
Preprint. Discussion started: 25 September 2019

463 directly before and after seasonal temperature maxima (**Fig. 8**). Finally, $\delta^{13}C$ values exhibit no observable
464 relationship with temperature seasonality.

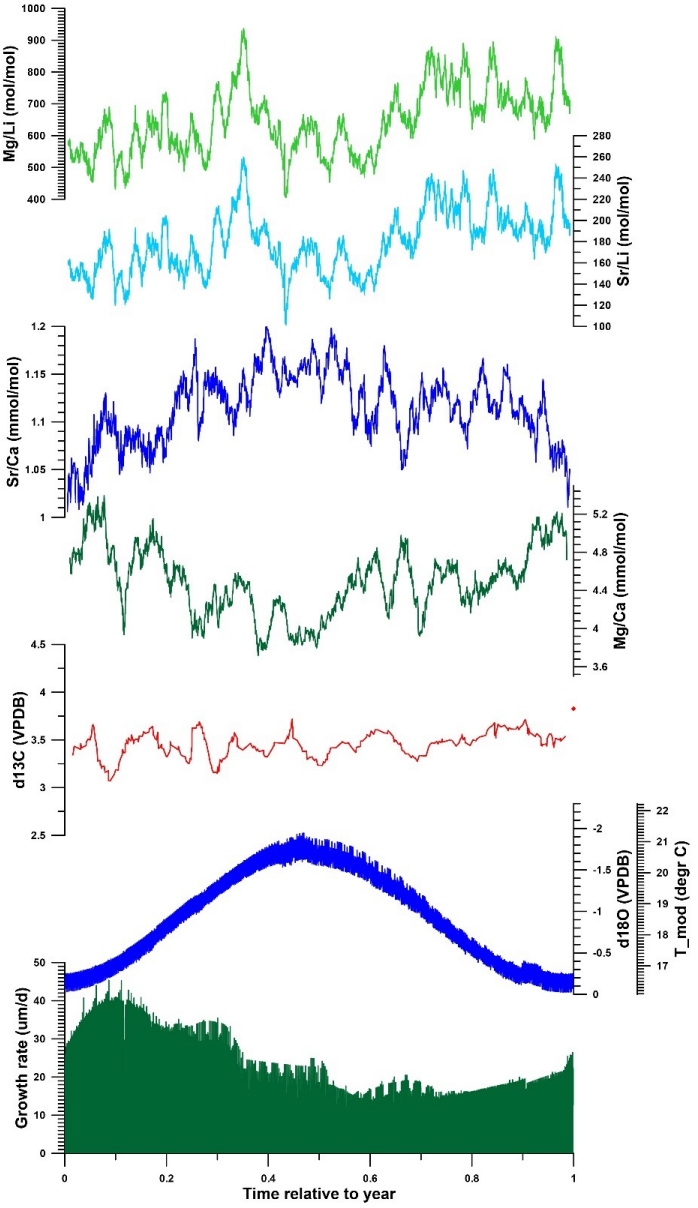

Figure 8: Composite of multi-proxy records from all *R. diluvianum* shells stacked and plotted on a common time axis of 1 year to illustrate the general phase relationships between various proxies in the shells. Records were colored as in **Fig. 6**. Annual stacks plotted in this figure were produced/obtained by applying age models on all multi-proxy records, plotting all results against their position relative to the annual cycle and applying 20 point moving averages.

465

466 3.8 Shell growth

https://doi.org/10.5194/bg-2019-74
Preprint. Discussion started: 25 September 2019

Biogeosciences Discussions Open Access EGU

Plots of modelled shell height against age allow to compare growth patterns of individual *R. diluvianum* (**Fig. 9**). Individual growth curves clearly converge to a general growth development curve for the species. Considering that the isotope transects used to establish these growth curves were measured in different stages of life in different specimens (large age variation), individual growth curves are remarkably similar. The growth of *R. diluvianum* takes the typical shape of the asymptotic Von Bertalanffy curve, in which shell height (H_t) development with age (t) is related to a theoretical adult size H_{max} and a constant k in the equation: $H_t[mm] = H_{max} * \left(1 - e^{k*(t[yr]-t_0)}\right)$, with t_0 representing the time at which the growth period started (always zero in this case; Von Bertalanffy, 1957). When this formula is regressed over all modelled growth data of all shells (1 data point per day, 15146 points in total), the fit with an H_{max} of ±120.3 mm and a K value of ±0.32 is very good (R^2 = 0.79; see **Fig. 9**).

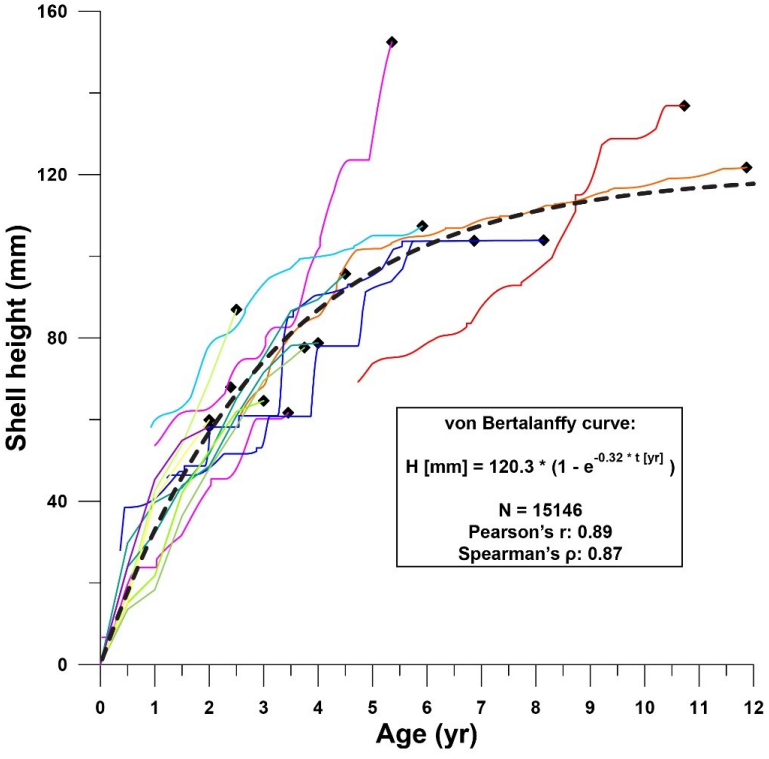

Figure 9: Shell height plotted against age for all *R. diluvianum* records (see **Fig. 7** for color legend of lines representing individuals). The similarity between growth curves of different specimens allows a Von Bertalanffy curve to be fitted to the data with high confidence. Sinusoidal patterns superimposed on all growth curves are caused by seasonal variability in growth rate (see **Fig. 6** for an example). Data found in **S9**.

3.9 Statistics in seasonal growth and ecology

The seasonality stack of growth rates shown in **Fig. 8** suggests a potential year-round growth in *R. diluvianum*, but this is a bias induced by the way the annual stack is plotted. To better understand the growth and life history of *R. diluvianum* oysters, it is important to consider the variability between individual years of growth in the different individuals. Using oxygen isotope records, year-long "seasonal" cycles and subsequently derived growth rates from our 12 specimens of *R. diluvianum*, we isolated statistics of individual growth seasons in order to visualize the potential relationship between growth rate, temperature and time of year (**Fig. 10**). The onset and end of each year correspond to maxima in $\delta^{18}O$ values (minima in temperatures). Isolating all 58 individual growth years in specimens used in this study based on the temperature seasonality modelled on $\delta^{18}O$ records allowed a comparison of statistics such as seasonal minima and maxima in growth, the length of the growth season and the extent of seasonality to be evaluated

https://doi.org/10.5194/bg-2019-74
Preprint. Discussion started: 25 September 2019

(**Fig. 10**). The onset of the first growth year in each shell at its precise position relative to the seasonal temperature cycle showed in which season spawning occurred (**Fig. 10c**). Finally, evaluation of the distribution of growth maxima and minima along the seasonal cycle and regression analyses between these parameters reconstructed from the growth models shed light on the relationships between growth parameters in *R. diluvianum* and seasonality All data used to create plots in **Fig. 10** is provided in **S14**.

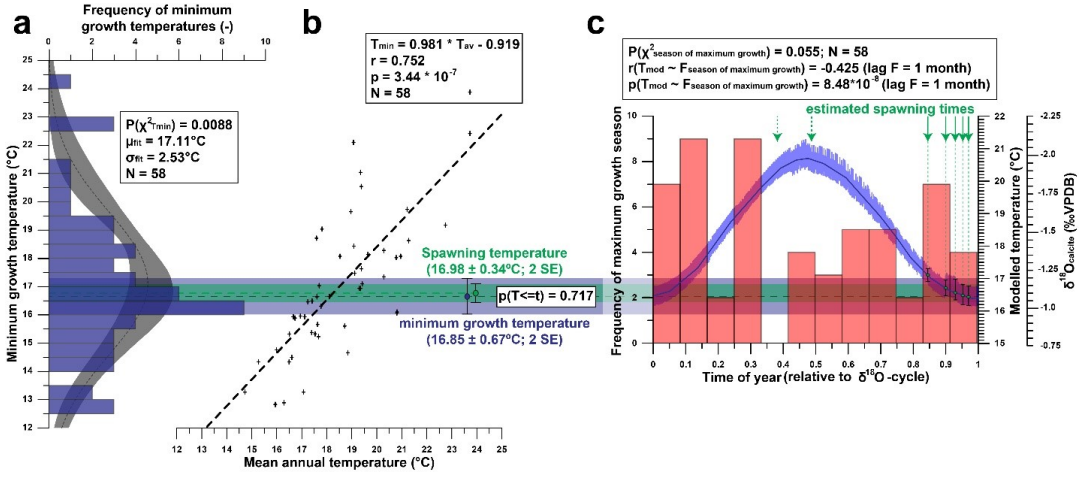

Figure 10: Overview of statistical evaluation of growth parameters of *R. diluvianum* derived from age modelling in shells 1-5. (**a**) Histogram of minimum temperatures of growth in *R. diluvianum* showing that the temperature on which growth slows coincides with that of the spawning season (p = 0.717). (**b**) Strong significant positive correlation between MAT and temperature of the slowest growth season shows that the season of minimum growth is not strictly forced by minimum temperatures but rather by timing relative to the annual $\delta^{18}O$ cycle. (**c**) Histogram of the season of maximum growth relative to the $\delta^{18}O$ seasonality cycle shows no significant concentration towards a favorable growing season while moments of first growth (spawning) are significantly concentrated towards the low-$\delta^{18}O$ season.

N = 58	Total annual growth (µm)	Maximum growth rate (µm/d)	Length of season (d)	Minimum growth temperature (°C)	Temperature seasonality (°C)	Average temperature (°C)
Temperature seasonality (°C)	R^2 0.024 p $2.16*10^{-11}$	R^2 0.053 p $6.73*10^{-10}$	R^2 0.403 p $2.15*10^{-22}$			
Average temperature (°C)	R^2 0.020 p $2.29*10^{-11}$	R^2 0.027 p $6.95*10^{-7}$	R^2 0.008 p $2.87*10^{-21}$	R^2 0.565 p $3.44*10^{-7}$		
Age (yr)	R^2 0.000 p $1.11*10^{-9}$	R^2 0.062 p $9.74*10^{-12}$	R^2 0.002 p $1.59*10^{-22}$	R^2 0.002 p $1.05*10^{-30}$	R^2 0.059 p $4.59*10^{-1}$	R^2 0.000 p $1.09*10^{-35}$

Table 2: Overview of statistical evaluation of growth parameters of *R. diluvianum* derived from age modelling in shells 1-5. Coefficients of determination (R^2) and p-values were determined for relationships between temperature seasonality, average temperature, age of the bivalve, length of the season, minimum growth temperatures and annual average and maximum growth rates. Values in green indicate strong correlations while values in red indicate the absence of a correlation. Data reported in **S14**.

4. Discussion

4.1 Preservation

The relative lack of burial and tectonic activity in the Kristianstad Basin has provided ideal circumstances for the nearly immaculate preservation of *R. diluvianum* shells in the Ivö Klack locality (Kominz et al., 2008; Surlyk and Sørensen, 2010). The excellent state of these shells is evident by the preservation of original (porous and foliated) microstructures that closely resemble those reported for several species of modern ostreid shells (Carriker et al., 1979; Surge et al., 2001; Ullmann et al., 2010; 2013; Zimmt et al., 2018; **Fig. 2-3**). High magnification SEM images demonstrate the excellent preservation of foliated and vesicular calcite structures in *R. diluvianum* shells (**Fig. 3b-d**). The preservation state of *R. diluvianum* shells meets the criteria for robust stable isotope analysis set by Cochran et al. (2010). MicroXRF mapping reveals that

https://doi.org/10.5194/bg-2019-74
Preprint. Discussion started: 25 September 2019

the foliated calcite in the shells is characterized by high Sr concentrations and low concentrations of Mn, Fe and Si, elements which are generally associated with diagenetic alteration (e.g. Brand and Veizer, 1980; Al-Aasm and Veizer, 1986a; Immenhauser et al., 2005; **Fig. 3b-h**). Typically, a Mn concentration threshold of 100 µg/g is applied below which Cretaceous low-magnesium carbonates are assumed suitable for chemical analysis (Steuber et al., 2005; Huck et al., 2011). Strontium concentrations above 1000 µg/g have also been used as markers for good preservation, since diagenetic processes can cause strontium to leach out of carbonates (e.g. Brand and Veizer, 1980; Huck et al., 2011; Ullmann and Korte, 2015). Therefore, previous studies of belemnites in Kristianstad Basin proposed a molar Sr/Mn threshold of 100 (Sørensen et al., 2015). However, maintaining thresholds for diagenetic screening is relatively arbitrary and the height of the thresholds used differs widely in the literature (e.g. Veizer, 1983; Steuber et al., 2002; Ullmann and Korte, 2015; de Winter and Claeys, 2016). Applying these thresholds risks introducing biases to chemical datasets from fossil shells and may not be an ideal method for diagenetic screening. Furthermore, large variation in the *in vivo* incorporation of Mn and Sr in mollusk shell carbonate and a strong dependence on the diagenetic setting can make the interpretation of shell preservation from trace element ratios alone highly ambiguous (Ullmann and Korte, 2015). This conclusion is supported by the trace element and stable isotope data gathered and compiled in this study (**Fig. 5**). Comparison of data from different fossil species in Ivö Klack with two closely related modern oyster species from different environments indicates that the differences between fossil mollusk species are similar to the differences among modern oyster species. It also shows that pristine carbonate from modern oyster shells can contain up to 200 µg/g Mn accompanied by a wide range in Sr concentrations.

One should be cautious when directly comparing trace element concentrations in biogenic calcite between different time periods, as seawater composition of Late Cretaceous oceans (e.g. concentrations of Mg, Ca, Sr and especially Li) may have been different from that of the present-day ocean (Stanley and Hardie, 1998; Coggon et al., 2010; Rausch et al., 2013). For this reason, one would expect, for example, that Sr concentrations in Late Cretaceous biogenic carbonate would be twice as low as those in carbonates formed in the modern ocean (Stanley and Hardie, 1998; de Winter et al., 2017a). Trends in Mn and Sr concentrations observed in all fossil species from Ivö Klack (**Fig. 5b**) likely point towards a diagenetic process affecting a subset of the data. When observing variations in $\delta^{18}O$ (a sensitive proxy for diagenesis and recrystallization; Brand and Veizer, 1980; Al-Aasm and Veizer, 1986b; **Fig. 5d**), the lack of covariation between Mn concentration and $\delta^{18}O$ shows that there is little evidence for meteoric diagenesis in these shells (Ullmann and Korte, 2015). Instead, these patterns are best explained by early marine cementation of porous carbonate structures from sea water with similar temperature and $\delta^{18}O$ as the living environment (see also Sørensen et al., 2015). These complex patterns merit great care in applying simple, general thresholds for diagenesis. Therefore, in this study, a multi-proxy approach is applied for diagenetic screening in which data is excluded based on a combination of Si, Ca, Mn, Fe and Sr concentrations, $\delta^{18}O$ values as well as SEM and visual observations of the shell structure at the location of measurement.

4.2 Dating of the Ivö Klack locality

Strontium isotope dating places the Ivö Klack deposits at 78.14 ± 0.26 Ma (**Fig. 4**). Nevertheless, age estimates from strontium isotope analyses could be biased towards a younger age due to the influx of radiogenic strontium-rich weathering products from the nearby Transscandinavian Igneous Belt (Högdal et al., 2004). This may explain the fact that, when plotting the obtained age of 78.14 Ma on the compilation by Wendler (2013), the age of the Ivö Klack falls slightly above the early/late Campanian subdivision (which is placed at ~78.5 Ma), while the *B. mammilatus* biozone is defined as late early Campanian. However, studies of modern strontium isotope ratio variability (Palmer and Edmond, 1989) and the potential bias of strontium isotope ratios in shallow-water carbonates (Kuznetsov et al., 2012; Meknassi et al., 2018) show that the effect of such inputs on strontium isotope dating results is generally negligible, except in semi-confined shallow-marine basins characterized by considerable freshwater input and low salinities (<7 g/kg). No evidence for such exceptional conditions at Ivö Klack exist (see **section 4.3**). We therefore conclude that our strontium isotope age estimate, together with biostratigraphic constraints, places the Ivö Klack locality in the latest early Campanian.

The refined dating of the Ivö Klack deposits and fossils allows the results of sclerochronological investigations presented in this work to be placed in the context of longer-term climate reconstructions with improved precision. While previous attempts at dating Campanian strata mainly focused on relative dating using magneto- and biostratigraphy (Montgomery et al., 1998; Jarvis et al., 2002; Voigt et al., 2010),

https://doi.org/10.5194/bg-2019-74
Preprint. Discussion started: 25 September 2019

integration of cyclostratigraphic approaches in this integrated stratigraphic framework has recently allowed to constrain the age of the Campanian deposits more precisely (Voigt and Schönfield, 2010; Thibault et al., 2012; Wendler, 2013; Thibault et al. 2016). Unfortunately, these attempts rarely cover the time interval in which the Ivö Klack sediments were deposited (latest Early Campanian; e.g. Wendler, 2013; Perdiou et al., 2016). Given the length of individual magnetochrons, carbon isotope shifts and biozones, the accuracy of dating obtained by strontium isotope dating cannot, at the moment, be matched by the abovementioned integrated stratigraphical approaches (Wagreich et al., 2012). For short, nearshore sections that cannot be replaced within a long-term stratigraphic framework (such as Ivö Klack), strontium isotope stratigraphy on well-preserved samples remains the most reliable dating method at present.

4.3 Ontogeny, metabolism and environment

The complex relationship between $\delta^{13}C$ and $\delta^{18}O$ records in *R. diluvianum* suggests that multiple factors influence the incorporation of carbon into the shell calcite. In marine mollusks, dissolved inorganic carbon (DIC) in the ambient sea water contributes to the majority (90%) of carbon used for shell mineralization (McConnaughey, 2003; Gillikin et al., 2007). However, changes in respiration rates can alter the carbon budget of shell carbonate by adding or removing isotopically-light respired carbon in the form of CO_2 (Lorrain et al., 2004). Of course, environmental changes in DIC can also have a strong influence on this carbon budget, especially when bivalves grow in nearshore or estuarine conditions with large (seasonal) variations in environmental $\delta^{13}C$ of DIC and organic carbon (Gillikin et al., 2006). Conceptual models exist that attempt to correlate shell $\delta^{13}C$ in modern mollusks to environmental and physiological variations, but these require knowledge of ambient CO_2 pressures and $\delta^{13}C$ values of DIC, gas ventilation rates in the animal and CO_2 and O_2 permeabilities of membranes (McConnaughey et al., 1997). Since these boundary conditions are not available in fossil bivalve studies, the following discussion will remain limited to qualitative interpretations of $\delta^{13}C$ trends.

A part of the variation in $\delta^{13}C$ may be explained by the presence of ontogenetic trends. These trends are known to occur in marine and freshwater bivalves as well as in bivalves with symbionts (Klein et al., 1996b; Watanabe et al., 2004; Gillikin et al., 2007; McConnaughey and Gillikin, 2008). The scale and direction of these trends in $\delta^{13}C$ are not consistent between individual *R. diluvianum* shells, which is also the case in other bivalve species (see **section 3.5**; McConnaughey and Gillikin, 2008 and references therein). Studies of modern bivalves show that in larger (older) bivalves, the contribution of respired CO_2 to carbon in the shell is larger (up to 40%; Gillikin et al., 2007). This finding explains common trends of reducing $\delta^{13}C$ with age in bivalve shells, since respired carbon is isotopically lighter than environmental DIC. Since ontogenetic trends are likely caused by changes in the amount of respired carbon entering the shell, and the direction of these trends in *R. diluvianum*, the contribution of respired CO_2 to *R. diluvianum* shells likely did not strictly increase with age. While this complicates the interpretation of $\delta^{13}C$ records, the relative contribution of environmental changes to $\delta^{13}C$ variability in *R. diluvianum* shells does appear to be highest on the positive end of the ontogenetic trend.

In all $\delta^{13}C$ records we observe that the parts of the record that exceed a $\delta^{13}C$ value of ±3.6‰ exhibit more regular variations of ±0.6‰ that are correlated to the seasonal variability in $\delta^{18}O$ (see **S6**). These periods of covariation between $\delta^{13}C$ and $\delta^{18}O$ do not dominate in the records, as is evident from the lack of seasonality in the annual stack of $\delta^{13}C$ (**Fig. 8**). It is possible that, during parts of the lifetime of *R. diluvianum* when the effect of respiration on $\delta^{13}C$ of the shell is reduced, $\delta^{13}C$ fluctuations reflect a combination of changes in DIC and/or salinity in the environment, which are likely paced to the seasonal cycle. These ±0.6‰ shifts in $\delta^{13}C$ that appear to be seasonal are much smaller than those in modern oyster records (2-3‰ in low-latitude estuarine *Crassostrea virginica*; Surge et al., 2001; 2003; Surge and Lohmann, 2008). Instead, the determined shifts more closely resemble the 0.5‰ variability in $\delta^{13}C$ observed in modern *Crassostrea gigas* from the same approximate latitude as Ivö Klack in the North Sea (Ullmann et al., 2013). The extreme isotopic shifts in the estuarine *C. virginica* specimens have been shown to be caused by large shifts in freshwater input due to large seasonal variations in rainfall over southern North America (Surge et al., 2003), while smaller variations in *C. gigas* from the North Sea are produced by DIC changes due to seasonal changes in productivity (e.g. spring blooms; Ullmann et al., 2013). The closer resemblance of *R. diluvianum* to the North Sea condition evidences that the Ivö Klack paleoenvironment did not experience large seasonal shifts in freshwater input and may have seen productivity peaks in spring season. The latter interpretation is in agreement with the coincidence of negative $\delta^{13}C$ excursions (in parts of the records not

https://doi.org/10.5194/bg-2019-74
Preprint. Discussion started: 25 September 2019

affected by ontogenetic trends and respiration) with the low-$\delta^{18}O$ season (winter or spring; **S6**) and the occurrence of spawning and a peak in growth rates in the spring season (much like in wild modern oysters; Berthelin et al., 2000; **Fig. 8,10a**). Large shifts in freshwater input are unlikely to have occurred in the Ivö Klack setting, lending more confidence to the growth and temperature modelling based on $\delta^{18}O$ records, which requires the assumption that changes in $\delta^{18}O_{seawater}$ did not exert dominant control on the $\delta^{18}O$ in shell carbonate.

4.4 Temperature seasonality

Modelling of seasonal changes in growth rate and temperature based on the $\delta^{18}O$ records in *R. diluvianum* yielded a MAT of 18.7°C with an average seasonal range of 5.2°C (**Fig. 8**). The reconstructed MAT is 7-8 degrees warmer than the present-day 10-12°C mean annual sea surface temperature in the North and Baltic seas at the same latitude (50-55°N; IRI/LDEO Climate Data Library, 2018). The MAT found in this study is similar to the MAT of the late early Campanian Boreal Chalk Sea waters of 17-19°C based on long-term reconstructions (Lowenstam and Epstein, 1954; Jenkyns et al., 2004; Friedrich et al., 2005; Thibault et al., 2016) and is slightly warmer than mean annual air temperatures reconstructed at the same paleolatitude (±15°C; Amiot et al., 2004). Averaging seasonality (**Fig. 8**) underestimates the extent of seasonality at Ivö Klack, because not all seasons contributing to the average have long growing seasons, which will reduce the average extent of seasonality. A more accurate estimate of the seasonal extent is obtained by calculating the seasonal range from the coolest winter temperatures (12.6°C in *R. diluvianum* 4; **SI10**) with the warmest recorded summer temperature (26°C in *R. diluvianum* 1; **S10** which yields a maximum seasonal sea surface temperature range of ±13.4°C. This is significantly less than the 16-20°C temperature seasonality that occurs in the present-day Baltic and North seas at the same latitude as Ivö Klack (IRI/LDEO Climate Data Library, 2018). Data on temperature seasonality in the Late Cretaceous is scarce, especially in high-latitude settings. However, comparison with data on Cretaceous seasonality between 15°N and 35°N paleolatitude (Steuber et al., 2005) shows that while MAT at 50°N was significantly lower than those at lower latitudes (18°C vs. 25-30°C respectively), the seasonal temperature range during cooler periods in the Late Cretaceous was remarkably similar between latitudes (10-15°C in subtropical latitudes vs. ±14°C in this study). This observation contrasts with the present-day situation in Northern Africa and Europe, in which seasonal temperature ranges are generally much higher in mid- to high-latitudes (30-50°N) than in lower latitudes (10-30°N; Prandle and Lane, 1995; Rayner, 2003; Locarnini et al., 2013; NOAA, 2018). Such seasonalities reconstructed from bivalve shells are not consistent with model predictions of an ice-free Cretaceous world, since those models predict both smaller seasonal temperature ranges and a shallower paleotemperature gradient (Barrera and Johnson, 1999; Hay and Floegel, 2012; Upchurch et al., 2015).

4.5 Trace element proxies

4.5.1 Mg/Ca

From the data in **Fig. 8,** it is evident that there is a positive correlation between Mg/Ca and $\delta^{18}O$, or a negative correlation between Mg/Ca and temperature. This correlation is opposite to the temperature-relationships found in modern oyster species (Surge and Lohmann, 2008; Mouchi et al., 2013; Ullmann et al., 2013). Furthermore, the difference between seasonally high and low Mg/Ca values is small (1.2 mmol/mol) compared to seasonal variability observed in modern oysters (4-10 mmol/mol; Surge and Lohmann, 2008; Mouchi et al., 2013) and the variability between specimens of *R. diluvianum* (>3 mmol/mol; **Fig. 7**). This dampening of the Mg/Ca cycle likely results from phase shifts between seasonal Mg/Ca cycles in different specimens, causing seasonal cyclicity in different years and individuals to partly cancel each other out in the annual stacks in **Fig. 8** (see **SI10**). These inconsistencies and the inverse temperature correlation compared to modern oyster species demonstrate that it is unlikely that Mg/Ca ratios in *R. diluvianum* are predominantly controlled by water temperatures. Mg/Ca ratios can therefore not be used as reliable temperature proxies in this species.

4.5.2 Sr/Ca

Previous studies on modern bivalve species indicate that Sr/Ca ratios are not a likely candidate for reconstructing temperature (Gillikin et al., 2005; Schöne et al., 2013; Ullmann et al., 2013). However, the negative seasonal correlation between $\delta^{18}O$ and Sr/Ca ratios (**Fig. 8**) suggests that there is at least some seasonal parameter influencing Sr incorporation into *R. diluvianum* shells. This correlation cannot be

https://doi.org/10.5194/bg-2019-74
Preprint. Discussion started: 25 September 2019

explained by classic diagenetic alteration of the shell, since this process would cause more negative $\delta^{18}O$ values to coincide with lower Sr concentrations (Brand and Veizer, 1980; Ullmann and Korte, 2015; Sørensen et al., 2015), while the opposite is observed here. Unlike the Mg/Ca seasonality, comparison between Sr/Ca variability in **Fig. 7** and **Fig. 8** shows that the seasonal variability in Sr/Ca is much less dampened by inter-specimen variability and that phase relationships between Sr/Ca and $\delta^{18}O$ are consistent between individuals (see also **S6**). The variability in Sr/Ca observed in foliate calcite in *R. diluvianum* resembles seasonal variability in the same microstructure in modern *Crassostrea gigas* oysters grown in a similar, though cooler, environment (see discussion in **section 4.3**) both in relation to the $\delta^{18}O$ cycle and in absolute Sr/Ca values (0.8-1.0 mmol/mol; Ullmann et al., 2013). This resemblance would support a similar explanation for *R. diluvianum* as was attributed to Sr/Ca ratios in *C. gigas*, namely that the proxy reflects seasonal changes in ambient sea water chemistry. There is some uncertainty as to whether sea water Sr/Ca ratios in the Late Cretaceous were lower than (Stanley and Hardie, 1998; Coggon et al., 2010) or similar to (Steuber and Veizer, 2002; Lear et al., 2003) those in the modern ocean. Local enrichments in seawater Sr concentrations at Ivö Klack driving increased Sr composition in *R. diluvianum* are unlikely, since Sr/Ca ratios exhibit only small (2-3%) lateral variability in the world's oceans (De Villiers, 1999). Therefore, the similarity in absolute calcite Sr/Ca ratios between modern *C. gigas* and Campanian *R. diluvianum* may demonstrate that *R. diluvianum* incorporated more Sr into its shell than modern oysters compensating for lower ambient Sr concentrations.

4.5.3 Li-proxies

While tentative temperature reconstructions based on Sr/Li and Mg/Li ratios (**Fig. 7**) appear consistent with those found using $\delta^{18}O$, the stack in **Figure 8** shows that these ratios do not correlate with the seasonal $\delta^{18}O$ cycle. Instead, it seems as if both Mg/Li and Sr/Li follow the same pattern with two maxima per annual cycle. This, together with the strong covariation between Mg/Li and Sr/Li, is inconsistent with the temperature dependence of these proxies (see **Fig. 7**). Instead, this covariation points to strong variations in Li concentrations in the shells as drivers for the observed variability. The negative correlation between Sr/Ca and Mg/Ca found in **Fig. 8** contradicts the inter-shell correlation between Mg/Li and Sr/Li found in **Fig. 7**. This shows that, when comparing proxy records between shells, it is important to apply reliable age models to correctly align the records such as the growth and age modelling approach applied in this study. The age model-based approach reliably visualizes correlations between proxies on a seasonal scale, while the approach of comparing seasonal averages and ranges of proxies (**Fig. 7**) puts more emphasis on absolute inter-shell differences in the expression of proxies. While the latter may be useful in detecting specimen-specific vital effects in trace element proxies (Freitas et al., 2008), the seasonally aligned comparison in **Fig. 8** more reliably reveals relationships between proxies and can be used to infer temperature dependence.

The inter-specimen comparison (**Fig. 7**) and the presence of randomly distributed ontogenetic trends in Li/Ca (see **section 3.5**) suggests that a large part of the variability in Mg/Li and Sr/Li is controlled by mechanisms that are local or even specimen-specific. The apparent occurrence of two peaks per year in these records (**Fig. 8**) shows that sub-annual changes in environment may contribute to the variability in Li-proxies in *R. diluvianum*. Riverine input can be a large source contributing to the dissolved Li budget in shallow marine systems (Huh et al., 1998; Misra and Froelich, 2012). Therefore, synchronous fluctuations in Mg/Li and Sr/Li ratios observed in **Fig. 8** may reflect changes in riverine input over the year. However, stable isotope ratios in *R. diluvianum* show no sign of large fluctuations in freshwater input (see **section 4.3**), so the effect of these potential influxes on the local Li budget must have been limited. Furthermore, dissolved Li in modern rivers strongly covaries with Mg and Sr, causing an increase in freshwater input to have a limited effect on Mg/Li and Sr/Li ratios (Huh et al., 1998; Brunskill et al., 2003). The observation that the inter-species variability in these proxies is much larger than the sub-annual variability (50-300 mol/mol for Sr/Li and 350-1000 mol/mol for Mg/Li between specimens compared to 120-260 mol/mol for Sr/Li and 450-900 mol/mol for Mg/Li within a year) indicates that the effect of sub-annual environmental change is likely to be small, and specimen-specific effects dominate. These complications prevent the use of Mg/Li and Sr/Li proxies for temperature reconstructions in *R. diluvianum*.

The complexity of interpreting trace element proxies in this study shows that the incorporation of Mg and Li into *R. diluvianum* was likely heavily biologically regulated. This result demonstrates that earlier successful attempts to establish calibration curves for Li- and Mg-based temperature proxies (e.g. Füllenbach et al.,

https://doi.org/10.5194/bg-2019-74
Preprint. Discussion started: 25 September 2019

2015; Dellinger et al., 2018) are probably strictly limited to bivalve species or close relatives. The same conclusion was also drawn by Dellinger et al. (2018) based on Li/Mg and Li isotope ratio measurements in biogenic carbonates. The lack of Mg/Li or Sr/Li calibrations in modern oyster shells limits the interpretation of results in this study and establishing such calibrations using modern oysters in cultured experiments may allow these proxies to be used for reconstructions from fossil oyster shells in the future.

4.6 Growth and life cycle

Modelling the growth of *R. diluvianum* shells based on $\delta^{18}O$ profiles (Judd et al., 2018) yields a lot of information about the growth and life cycle of these oysters (**Fig. 9-10**). One of the most interesting results is the remarkable similarity in growth patterns between individuals of *R. diluvianum* (**Fig. 9**). Except for the final parts of growth curves of some of the older shells, all shells show similar development of shell height with age. This development is well approximated by a Von Bertalanffy curve with a K value of 0.32 and a theoretical full-grown shell height (H_{max}) of 120.3 mm ($r = 0.89$; $\rho = 0.87$; Von Bertalanffy, 1957; **Fig. 9**). The consistency in growth curves between individuals of *R. diluvianum* is somewhat surprising given the fact that modern oyster species are known to exhibit large variations in growth rates and shell shapes as a function of their colonial lifestyle, which often limits the growth of their shells in several directions (Galtsoff, 1964; Palmer and Carriker, 1979). The strong resemblance of growth between individuals and the close fit of the idealized Von Bertalanffy growth model suggests that growth of *R. diluvianum* at Ivö Klack was relatively unrestricted in space. This hypothesis is consistent with the apparent mode of life of *R. diluvianum* in Ivö Klack cemented together in groups, subject to strong wave action and turbulence, but with little competition for space due to the high-energy environment (Surlyk and Christensen, 1974; Sørensen et al., 2012). The shape of the growth curve of *R. diluvianum* is fairly consistent with that of modern Chesapeake Bay oysters (*Crassostrea virginica*), which exhibit a slightly larger modelled maximum height (150 mm) and a slightly smaller K-value (0.28). A larger subset of *R. diluvianum* specimens studied by Sørensen et al. (2012) demonstrates that these bivalves could grow up to 160 mm in height. The curvature of the growth of *R. diluvianum* (K -value) is also similar to that found for other modern shallow marine bivalve species (e.g. *Macoma balthica*, K = 0.2-0.4; Bachelet, 1980; *Pinna nobilis*, K = 0.33-0.37; Richardson et al., 2004) and significantly higher than in growth curves of deep marine bivalves (e.g. *Placopecten magellanicus*, K = 0.16-0.24; MacDonald and Thompson, 1985; Hart and Chute, 2009) or bivalves from cold habitats (e.g. North Atlantic *Arctica islandica*, K = 0.06; Strahl et al., 2007). This reflects the high growth rates (steeper growth curves, higher K-values) of shallow marine bivalves compared to species living in more unfavorable or restricting (colder or deeper) habitats, with *R. diluvianum* clearly being part of the former group.

Figure 10 and **Table 2** illustrate statistics of growth and seasonality for a total of 58 years of growth in the complete dataset. This data indicates that the growing season is shorter than 365 days in all but five modelled years, demonstrating that growth stops did occur in *R. diluvianum*. Minimum growth temperatures (temperatures by which growth stops) are concentrated around 17°C ($\chi^2 = 0.0088$; **Fig. 10a**) and correlate strongly to MAT (Pearson's $r = 0.752$; **Fig. 10b**), suggesting that while potential growth halts in *R. diluvianum* occur systematically at a certain time interval of the year (first half of "winter"), they are not forced by an absolute temperature threshold, but rather by timing relative to the seasonality (circadian rhythm). On average, the moment of minimum growth occurs right after the highest temperatures of the year are reached (early autumn, **Fig. 8**).

The spawning season (onset of the first growth year, see **3.9**) is concentrated in the two last months before the $\delta^{18}O$ maximum (first half of "winter") when modelled water temperatures are ±17°C (**Fig. 10c**). Note that only three of the five shells allowed sampling of the first month of growth, and extrapolated records for the other two shells yielded spawning around the $\delta^{18}O$ minimum ("summer"). The offset of these estimates likely results from uncertainty introduced due to extrapolation of the records of these two remaining shells, showing that these estimates are likely unreliable. Comparing **Fig. 10c** and **Fig. 10a** shows that growth halts and spawning occur at similar temperatures (16.85 ± 0.67°C and 16.98 ± 0.34°C respectively, $p = 0.717$), suggesting that these events occur simultaneously or on either side of a seasonal growth halt (if it occurs).

Figure 10c shows that the distribution of months with fastest growth rate is random ($p(\chi^2) = 0.055$, <95% confidence). However, in 27 of the 58 years, the growth peak occurs in the season with decreasing $\delta^{18}O$ values ("spring season"), just after the moment of spawning (winter season; **Fig. 10a-b**). **Table 2** shows that the extent of temperature seasonality (difference between minimum and maximum $\delta^{18}O$ converted to

https://doi.org/10.5194/bg-2019-74
Preprint. Discussion started: 25 September 2019

temperature) significantly influences the length of the growing season (strong correlation), the maximum growth in that year and the total annual growth (weak correlations). MAT is a weak but significant driver of annual growth, maximum growth and length of growing season. Ontogenetic age of the organism does not predict a significant part of any of the above mentioned growth and seasonality parameters (**Table 2**). All this suggests that temperature seasonality may not have been the dominant factor causing growth cessations in *R. diluvianum*. This hypothesis is supported by the observation that temperatures at which growth cessations occur (16.85 ± 0.67°C; **Fig. 10b**) show large variability and do not correspond significantly to the lowest temperatures of the year.

This pattern is decidedly different from that observed in modern *Crassostrea gigas* shells, which generally stop growing their shell at temperatures below ±10°C (Surge et al., 2001; Lartaud et al., 2010; Ullmann et al., 2013). In contrast, lower latitude *Crassostrea virginica* from estuarine environments cease shell growth at temperature maxima (>28°C; Surge et al., 2001). Other bivalves are known to have more flexible temperature thresholds for shell precipitation (Ivany, 2012), but a lack of correlation between shell age and length of season or minimum growth temperature (**Table 2**) demonstrates that there is no evidence for this in *R. diluvianum*. These observations do not necessarily show that *R. diluvianum* tolerated larger temperature differences than these modern taxa, because the maximum extent of seasonality between 12.6°C and 26°C reconstructed from $\delta^{18}O$ records in this study (see **section 4.3**) causes neither the lower nor the upper limit of temperature tolerance in modern oysters to be reached. If temperature tolerance of *R. diluvianum* did resemble that of its closest modern relatives, then the mild seasonal temperature cycle at Ivö Klack might have provided the ideal temperature conditions for its growth. Perhaps these favorable conditions partly explain why biodiversity and abundance of invertebrates at Ivö Klack was so high (Surlyk and Sørensen, 2010). If this was the case, then shell growth in *R. diluvianum* may not have been governed by temperature, but rather by changes in productivity, as was already hypothesized based on fluctuations in $\delta^{13}C$ (see **section 4.4**). A strong 1:1 correlation between MAT and the temperature by which growth cessations occur (slope = 0.981; r = 0.752; **Fig. 10c**) supports the hypothesis that absolute temperatures did not limit shell growth, but rather that growth cessations occur consistently in certain parts of the seasonal cycle. The observation that peak growth rates and spawning both occur during the early spring season (**Fig. 10c**) is also consistent with the occurrence of spring blooms of increased productivity (**section 4.3**).

Finally, as **Table 2** shows, the length of the growing season positively correlates with the size of temperature seasonality. This relationship is opposite to what would be expected if temperature controlled the growth of *R. diluvianum* shells, since in that case, larger temperature seasonality would cause intolerable temperature thresholds to be reached during larger parts of the seasonal cycle, which would shorten the length of the growing season. Instead, the correlation in **Table 2** can be explained by a small input of isotopically light freshwater in spring carrying nutrients to initiate the spring bloom (Arthur et al., 1983; Krantz et al., 1987). Such a freshwater contribution would reduce $\delta^{18}O_{seawater}$ in the early spring season and dampen the seasonality in shell $\delta^{18}O$ values. A larger influence of seasonal freshwater input would cause longer growth cessations to occur in the spring season, reducing the length of the growing season while also dampening the reconstructed temperature seasonality, which explains the correlation found between these two parameters. At the same time, this freshwater input would increase reconstructed MAT by increasing $\delta^{18}O$ values in *R. diluvianum* shells, explaining the weak positive correlation between MAT and length of the growing season (**Table 2**). While seasonal changes in salinity and seawater $\delta^{18}O$ must have remained limited at Ivö Klack (see **section 4.3**), from the discussion above we conclude that seasonal differences in productivity, potentially forced by input of nutrient-rich freshwater, are likely to have been a major factor influencing shell growth in *R. diluvianum* at Ivö Klack. In this case, dampening of the seasonal $\delta^{18}O$ cycle may cause temperature seasonality reconstructions in this study to underestimate the real extent of seasonality.

5. Conclusions

The highly biodiverse marine invertebrate community at Ivö Klack in the Kristianstad Basin in southern Sweden offers a unique opportunity to recover a wealth of information about Campanian climate and environment in high latitudes and the ecology and life of extinct invertebrate species that lived under these conditions. The lack of burial and tectonic activity in the region favored *Rastellum diluvianum* fossil shells from Ivö Klack to be well preserved, as is evident from the excellent preservation of growth structures typical

https://doi.org/10.5194/bg-2019-74
Preprint. Discussion started: 25 September 2019

for ostreid shells as well as from limited evidence for geochemical changes associated with diagenetic alteration. This excellent preservation allows the shells of *R. diluvianum* to be used to accurately and precisely constrain the age of the Ivö Klack locality using strontium isotope stratigraphy (78.14 ± 0.26 Ma). Furthermore, *R. diluvianum* shells reveal sub-annual scale variability in temperature, local environment and growth rates through our multi-proxy geochemical approach. The combination of trace element and stable isotope measurements with growth modelling based on $\delta^{18}O$ records in the shells allow all measured proxies to be aligned on the same time axis. Application of transfer functions for potential Mg/Ca, Mg/Li and Sr/Li temperature proxies established in modern invertebrates yields temperatures consistent with those calculated from $\delta^{18}O$ records. However, close examination of the seasonal phase relationships between these proxies reveals that the sub-annual variability in these trace element ratios is not controlled by temperature changes alone. This observation supports previous studies that found the expression of trace element proxies to be highly variable among species and even among different specimens of the same species. If trace element proxies are to be used for seasonality reconstructions in pre-Quarternary times, a more robust, non-species-specific model for the incorporation of trace elements by bivalves is required. Establishing such a model requires culture experiments with different bivalve species in which multiple parameters influencing trace element composition can be controlled (e.g. temperature, salinity, food intake and microstructure).

Stable isotope records in *R. diluvianum* shells reveal a MAT of 17-19°C with a maximal seasonal water temperature range of ±14°C (12.6°C - 26°C) at Ivö Klack. This value for MAT is consistent with long-term temperature reconstructions in the Campanian Boreal Chalk Sea. Comparing the seasonal temperature range reconstructed from *R. diluvianum* shells with other Late Cretaceous seasonality records from lower latitudes reveals that temperature seasonality was remarkably similar across latitudes. These reconstructions contradict results from climate models, which predict smaller temperature seasonalities. This disagreement between data and models clearly illustrates the disadvantage of the lack of data on Late Cretaceous seasonality outside the (sub-)tropical latitudes and highlights how important such reconstructions are for improving our understanding of the dynamics in temperature variability in both space and time during greenhouse climates.

Finally, the coupled modelling and multi-proxy approach applied in this study sheds light on the effects of environmental changes on the life cycle and sub-annual growth of *R. diluvianum* shells. This study reveals that growth curves of *R. diluvianum* strongly resemble those in modern shallow marine bivalves that grow in coastal high latitude environments. However, changes in growth rate of our Boreal oysters seem unrelated to temperature, in contrast to modern, high-latitude oysters that tend to lower their growth rate and cease mineralization below a certain cold threshold. We conclude that growth cessations and sub-annual changes in growth rate in *R. diluvianum* were most likely not caused by intolerable temperatures, but rather by circadian rhythm tied to the seasonal cycle and seasonal changes in sea surface productivity, driven by nutrient-rich freshwater inputs.

Acknowledgements

This work was made possible with help of a IWT doctoral fellowship (IWT700) awarded to Niels de Winter. Instrumentation at the VUB was funded by Hercules infrastructure grants (HERC9 and HERC1309). The authors acknowledge financial and logistic support from the Flemish Research Foundation (FWO, research project G017217N) and Teledyne CETAC Technologies (Omaha, NE, USA) as well as support from VUB Strategic Research (BAS48). Stijn Goolaerts is funded by a Belspo Brain project (BR/175/A2/CHICXULUB). The authors would like to thank David Verstraeten for his help with stable isotope analyses. We thank Bart Lippens for assisting sample preparation and Joke Belza for help with the LA-ICP-MS analyses. Thanks are due to Julien Cilis for his assistance with SEM imaging. The authors wish to thank Emily Judd for discussions about her growth rate model for bivalve shells and Roger Barlow for his assistance with combining strontium isotope measurements with asymmetric error distributions.

https://doi.org/10.5194/bg-2019-74
Preprint. Discussion started: 25 September 2019

Biogeosciences Discussions Open Access EGU

Supplementary files

All supplementary files are stored in the open access online database Zenodo and can be accessed using the following link: **https://zenodo.org/record/2581305**

S1: High resolution (6400 dpi) scans of cross sections through the 12 shells of *Rastellum diluvianum* used in this study.
S2: Compilation of µXRF maps of cross sections through the 12 shells of *Rastellum diluvianum* used in this study.
S3: Compilation of XRF line scans measured through the foliated calcite of *Rastellum diluvianum* shells.
S4: Compilation of LA-ICP-MS data collected within the context of this study.
S5: Compilation of IRMS data used in this study.
S6: Composite figures of XRF linescan data through the shells of *Rastellum diluvianum*.
S7: Source code of the bivalve growth model adapted from Judd et al. (2018) including temperature equations for calcite.
S8: Compilation of strontium isotope data and ages used in this study.
S9: Compilation of the results from growth modelling on 5 *Rastellum diluvianum* shells.
S10: Compilation figures of proxy record data plotted on time axis for all 5 shells for which modelling was carried out.
S11: Plot of ontogenetic trends in $\delta^{13}C$ and Li/Ca proxies including statistics on the spread of the slopes of these trends.
S12: Data on trends in $\delta^{13}C$ and Li/Ca.
S13: Data used to create seasonality crossplots shown in **Fig. 7**.
S14: Data on statistics of the growth rates, seasonality and spawning season of all 5 bivalves for which modelling was done.

References

Al-Aasm, I.S., Veizer, J.: Diagenetic stabilization of aragonite and low-Mg calcite, I. Trace elements in rudists. Journal of Sedimentary Research 56, 138–152, 1986a.
Al-Aasm, I.S., Veizer, J.: Diagenetic stabilization of aragonite and low-Mg calcite, II. Stable isotopes in rudists. Journal of Sedimentary Research 56, 763–770, 1986b.
Alberti, M., Fürsich, F.T., Abdelhady, A.A., Andersen, N.: Middle to Late Jurassic equatorial seawater temperatures and latitudinal temperature gradients based on stable isotopes of brachiopods and oysters from Gebel Maghara, Egypt. Palaeogeography, Palaeoclimatology, Palaeoecology 468, 301–313. https://doi.org/10.1016/j.palaeo.2016.11.052, 2017.
Amiot, R., Lécuyer, C., Buffetaut, E., Fluteau, F., Legendre, S., Martineau, F.: Latitudinal temperature gradient during the Cretaceous Upper Campanian–Middle Maastrichtian: $\delta^{18}O$ record of continental vertebrates. Earth and Planetary Science Letters 226, 255–272. https://doi.org/10.1016/j.epsl.2004.07.015, 2004.
Arthur, M.A., Williams, D.F., Jones, D.S.: Seasonal temperature-salinity changes and thermocline development in the mid-Atlantic Bight as recorded by the isotopic composition of bivalves. Geology 11, 655–659. https://doi.org/10.1130/0091-7613(1983)11<655:STCATD>2.0.CO;2, 1983.
Bachelet, G.: Growth and recruitment of the tellinid bivalve *Macoma balthica* at the southern limit of its geographical distribution, the Gironde estuary (SW France). Marine Biology 59, 105–117, 1980.
Barlow, R.: Asymmetric errors. arXiv preprint physics/0401042, 2004.
Barlow, R.: Asymmetric systematic errors. arXiv preprint physics/0306138, 2003.
Barrera, E., Johnson, C.C.: Evolution of the Cretaceous Ocean-climate System. Geological Society of America, 1999.
Berthelin, C., Kellner, K., Mathieu, M.: Storage metabolism in the Pacific oyster (*Crassostrea gigas*) in relation to summer mortalities and reproductive cycle (West Coast of France). Comparative Biochemistry and Physiology Part B: Biochemistry and Molecular Biology 125, 359–369. https://doi.org/10.1016/S0305-0491(99)00187-X, 2000.
Brady, E.C., DeConto, R.M., Thompson, S.L.: Deep water formation and poleward ocean heat transport in the warm climate extreme of the Cretaceous (80 Ma). Geophysical Research Letters 25, 4205–4208, 1998.
Brand, U., Veizer, J.: Chemical diagenesis of a multicomponent carbonate system-2: stable isotopes. Journal of Sedimentary Research 51, 987–997, 1981.
Brand, U., Veizer, J.: Chemical diagenesis of a multicomponent carbonate system–1: Trace elements. Journal of Sedimentary Research 50, 1219–1236, 1980.
Brunskill, G.J., Zagorskis, I., Pfitzner, J.: Geochemical mass balance for lithium, boron, and strontium in the Gulf of Papua, Papua New Guinea (project TROPICS). Geochimica et Cosmochimica Acta 67, 3365–3383. https://doi.org/10.1016/S0016-7037(02)01410-2, 2003.
Bryan, S.P., Marchitto, T.M.: Mg/Ca–temperature proxy in benthic foraminifera: New calibrations from the Florida Straits and a hypothesis regarding Mg/Li. Paleoceanography 23, PA2220. https://doi.org/10.1029/2007PA001553, 2008.
Burgener, L., Hyland, E., Huntington, K.W., Kelson, J.R., Sewall, J.O.: Revisiting the equable climate problem during the Late Cretaceous greenhouse using paleosol carbonate clumped isotope temperatures from the Campanian of the Western Interior

https://doi.org/10.5194/bg-2019-74
Preprint. Discussion started: 25 September 2019

Basin, USA. Palaeogeography, Palaeoclimatology, Palaeoecology 516, 244–267. https://doi.org/10.1016/j.palaeo.2018.12.004, 2018.
Carriker, M.R., Palmer, R.E., Prezant, R.S.: Functional ultramorphology of the dissoconch valves of the oyster *Crassostrea virginica*, in: Proceedings of the National Shellfisheries Association. pp. 139–183, 1979.
Carriker, M.R., Swann, C.P., Prezant, R.S., Counts, C.L.: Chemical elements in the aragonitic and calcitic microstructural groups of shell of the oyster *Crassostrea virginica*: A proton probe study. Marine Biology 109, 287–297, 1991.
Christensen, W.K.: Paleobiogeography and migration in the Late Cretaceous belemnite family Belemnitellidae. Acta palaeontologica polonica 42, 457–495, 1997.
Christensen, W.K.: The Albian to Maastrichtian of southern Sweden and Bornholm, Denmark: a review. Cretaceous Research 5, 313–327, 1984.
Christensen, W.K.: Upper Cretaceous belemnites from the Kristianstad area in Scania. Fossils and Strata, 1975.
Clarke, L.J., Jenkyns, H.C.: New oxygen isotope evidence for long-term Cretaceous climatic change in the Southern Hemisphere. Geology 27, 699–702, 1999.
Cochran, J.K., Kallenberg, K., Landman, N.H., Harries, P.J., Weinreb, D., Turekian, K.K., Beck, A.J., Cobban, W.A.: Effect of diagenesis on the Sr, O, and C isotope composition of late Cretaceous mollusks from the Western Interior Seaway of North America. American Journal of Science 310, 69–88. https://doi.org/10.2475/02.2010.01, 2010.
Coggon, R.M., Teagle, D.A., Smith-Duque, C.E., Alt, J.C., Cooper, M.J.: Reconstructing past seawater Mg/Ca and Sr/Ca from mid-ocean ridge flank calcium carbonate veins. Science 327, 1114–1117, 2010.
Csiki-Sava, Z., Buffetaut, E., Ősi, A., Pereda-Suberbiola, X., Brusatte, S.L.: Island life in the Cretaceous - faunal composition, biogeography, evolution, and extinction of land-living vertebrates on the Late Cretaceous European archipelago. Zookeys 1–161. https://doi.org/10.3897/zookeys.469.8439, 2015.
Dalbeck, P., England, J., Cusack, M., Lee, M.R., Fallick, A.E.: Crystallography and chemistry of the calcium carbonate polymorph switch in *M. edulis* shells. European Journal of Mineralogy 18, 601–609. https://doi.org/10.1127/0935-1221/2006/0018-0601, 2006.
De Villiers, S.: Seawater strontium and Sr/Ca variability in the Atlantic and Pacific oceans. Earth and Planetary Science Letters 171, 623–634, 1999.
de Winter, N.J., Claeys, P.: Micro X-ray fluorescence (μXRF) line scanning on Cretaceous rudist bivalves: A new method for reproducible trace element profiles in bivalve calcite. Sedimentology 64, 231–251. https://doi.org/10.1111/sed.12299, 2016.
de Winter, N.J., Goderis, S., Dehairs, F., Jagt, J.W., Fraaije, R.H., Van Malderen, S.J., Vanhaecke, F., Claeys, P.: Tropical seasonality in the late Campanian (late Cretaceous): Comparison between multiproxy records from three bivalve taxa from Oman. Palaeogeography, Palaeoclimatology, Palaeoecology 485, 740–760, 2017a.
de Winter, N.J., Sinnesael, M., Makarona, C., Vansteenberge, S., Claeys, P.: Trace element analyses of carbonates using portable and micro-X-ray fluorescence: performance and optimization of measurement parameters and strategies. Journal of Analytical Atomic Spectrometry 32, 1211–1223, 2017b.
de Winter, N.J., Vellekoop, J., Vorsselmans, R., Golreihan, A., Soete, J., Petersen, S.V., Meyer, K.W., Casadio, S., Speijer, R.P., Claeys, P.: An assessment of latest Cretaceous *Pycnodonte vesicularis* (Lamarck, 1806) shells as records for palaeoseasonality: a multi-proxy investigation. Climate of the Past 14, 725–749, 2018.
de Winter, N.J., Goderis, S., Van Malderen, S.J.M., Sinnesael, M., Vansteenberge, S., Snoeck, C., Belza, J., Vanhaecke, F., Claeys, P., Daily chemical variability in a Late Cretaceous rudist shell. Science Advances, in review.
DeConto, R.M., Hay, W.W., Thompson, S.L., Bergengren, J.: Late Cretaceous climate and vegetation interactions: cold continental interior paradox. SPECIAL PAPERS-GEOLOGICAL SOCIETY OF AMERICA 391–406, 1999.
Dellinger, M., West, A.J., Paris, G., Adkins, J.F., von Strandmann, P.A.P., Ullmann, C.V., Eagle, R.A., Freitas, P., Bagard, M.-L., Ries, J.B.: The Li isotope composition of marine biogenic carbonates: Patterns and Mechanisms. Geochimica et Cosmochimica Acta 236, 315–335, 2018.
Donnadieu, Y., Pucéat, E., Moiroud, M., Guillocheau, F., Deconinck, J.-F.: A better-ventilated ocean triggered by Late Cretaceous changes in continental configuration. Nature Communications 7, 10316. https://doi.org/10.1038/ncomms10316, 2016.
Freitas, P.S., Clarke, L.J., Kennedy, H.A., Richardson, C.A.: Inter-and intra-specimen variability masks reliable temperature control on shell Mg/Ca ratios in laboratory and field cultured *Mytilus edulis* and *Pecten maximus* (bivalvia). Biogeosciences Discussions 5, 531–572, 2008.
Friedrich, O., Herrle, J.O., Hemleben, C.: Climatic changes in the late Campanian—early Maastrichtian: Micropaleontological and stable isotopic evidence from an epicontinental sea. Journal of Foraminiferal Research 35, 228–247, 2005.
Friedrich, O., Herrle, J.O., Wilson, P.A., Cooper, M.J., Erbacher, J., Hemleben, C.: Early Maastrichtian carbon cycle perturbation and cooling event: Implications from the South Atlantic Ocean. Paleoceanography 24, PA2211. https://doi.org/10.1029/2008PA001654, 2009.
Friedrich, O., Norris, R.D., Erbacher, J.: Evolution of middle to Late Cretaceous oceans—a 55 my record of Earth's temperature and carbon cycle. Geology 40, 107–110, 2012.
Füllenbach, C.S., Schöne, B.R., Mertz-Kraus, R.: Strontium/lithium ratio in aragonitic shells of *Cerastoderma edule* (Bivalvia)—A new potential temperature proxy for brackish environments. Chemical Geology 417, 341–355, 2015.
Galtsoff, P.S.: The American Oyster: US Fish and Wildlife Service. Fishery Bulletin 64, 480, 1964.
Gillikin, D.P., Lorrain, A., Bouillon, S., Willenz, P., Dehairs, F.: Stable carbon isotopic composition of *Mytilus edulis* shells: relation to metabolism, salinity, $\delta^{13}C$ DIC and phytoplankton. Organic Geochemistry 37, 1371–1382, 2006.
Gillikin, D.P., Lorrain, A., Meng, L., Dehairs, F.: A large metabolic carbon contribution to the $\delta^{13}C$ record in marine aragonitic bivalve shells. Geochimica et Cosmochimica Acta 71, 2936–2946, 2007.
Gillikin, D.P., Lorrain, A., Navez, J., Taylor, J.W., André, L., Keppens, E., Baeyens, W., Dehairs, F.: Strong biological controls on Sr/Ca ratios in aragonitic marine bivalve shells. Geochemistry, Geophysics, Geosystems 6, Q05009, 2005.
Goodwin, D.H., Flessa, K.W., Schone, B.R., Dettman, D.L.: Cross-calibration of daily growth increments, stable isotope variation, and temperature in the Gulf of California bivalve mollusk *Chione cortezi*: implications for paleoenvironmental analysis. Palaios 16, 387–398, 2001.
Grossman, E.L., Ku, T.-L.: Oxygen and carbon isotope fractionation in biogenic aragonite: temperature effects. Chemical Geology: Isotope Geoscience section 59, 59–74, 1986.

Hay, W.W., Floegel, S.: New thoughts about the Cretaceous climate and oceans. Earth-Science Reviews 115, 262–272, 2012.
Huber, B.T., Hodell, D.A., Hamilton, C.P.: Middle–Late Cretaceous climate of the southern high latitudes: stable isotopic evidence for minimal equator-to-pole thermal gradients. Geological Society of America Bulletin 107, 1164–1191, 1995.
Huber, B.T., Norris, R.D., MacLeod, K.G.: Deep-sea paleotemperature record of extreme warmth during the Cretaceous. Geology 30, 123–126, 2002.
Huck, S., Heimhofer, U., Rameil, N., Bodin, S., Immenhauser, A.: Strontium and carbon-isotope chronostratigraphy of Barremian–Aptian shoal-water carbonates: Northern Tethyan platform drowning predates OAE 1a. Earth and Planetary Science Letters 304, 547–558. https://doi.org/10.1016/j.epsl.2011.02.031, 2011.
Huh, Y., Chan, L.-H., Zhang, L., Edmond, J.M.: Lithium and its isotopes in major world rivers: implications for weathering and the oceanic budget. Geochimica et Cosmochimica Acta 62, 2039–2051. https://doi.org/10.1016/S0016-7037(98)00126-4, 1998.
Immenhauser, A., Nägler, T.F., Steuber, T., Hippler, D.: A critical assessment of mollusk $^{18}O/^{16}O$, Mg/Ca, and $^{44}Ca/^{40}Ca$ ratios as proxies for Cretaceous seawater temperature seasonality. Palaeogeography, Palaeoclimatology, Palaeoecology 215, 221–237, 2005.
IPCC: Climate Change 2013: The Physical Science Basis. Contribution of Working Group I to the Fifth Assessment Report of the Intergovernmental Panel on Climate Change, 1535 pp. Cambridge Univ. Press, Cambridge, UK, and New York, 2013.
IRI/LDEO Climate Data Library URL http://iridl.ldeo.columbia.edu (accessed 01/11/19).
Ivany, L.C.: Reconstructing paleoseasonality from accretionary skeletal carbonates—challenges and opportunities. The Paleontological Society Papers 18, 133–166, 2012.
Jablonski, D., Huang, S., Roy, K., Valentine, J.W.: Shaping the latitudinal diversity gradient: new perspectives from a synthesis of paleobiology and biogeography. The American Naturalist 189, 1–12, 2017.
Jenkyns, H.C., Forster, A., Schouten, S., Damsté, J.S.S.: High temperatures in the late Cretaceous Arctic Ocean. Nature 432, 888, 2004.
Jenkyns, H.C., Gale, A.S., Corfield, R.M.: Carbon-and oxygen-isotope stratigraphy of the English Chalk and Italian Scaglia and its palaeoclimatic significance. Geological Magazine 131, 1–34, 1994.
Jones, D.S.: Sclerochronology: reading the record of the molluscan shell: annual growth increments in the shells of bivalve molluscs record marine climatic changes and reveal surprising longevity. American Scientist 71, 384–391, 1983.
Judd, E.J., Wilkinson, B.H., Ivany, L.C.: The life and time of clams: Derivation of intra-annual growth rates from high-resolution oxygen isotope profiles. Palaeogeography, Palaeoclimatology, Palaeoecology 490, 70–83, 2018.
Kawaguchi, T., Watabe, N.: The organic matrices of the shell of the American oyster *Crassostrea virginica* Gmelin. Journal of Experimental Marine Biology and Ecology 170, 11–28. https://doi.org/10.1016/0022-0981(93)90126-9, 1993.
Kim, S.-T., O'Neil, J.R.: Equilibrium and nonequilibrium oxygen isotope effects in synthetic carbonates. Geochimica et Cosmochimica Acta 61, 3461–3475, 1997.
Klein, R.T., Lohmann, K.C., Thayer, C.W.: Bivalve skeletons record sea-surface temperature and $\delta^{18}O$ via Mg/Ca and $^{18}O/^{16}O$ ratios. Geology 24, 415–418, 1996a.
Klein, R.T., Lohmann, K.C., Thayer, C.W.: Sr/Ca and $^{13}C/^{12}C$ ratios in skeletal calcite of *Mytilus trossulus*: Covariation with metabolic rate, salinity, and carbon isotopic composition of seawater. Geochimica et Cosmochimica Acta 60, 4207–4221. https://doi.org/10.1016/S0016-7037(96)00232-3, 1996b.
Kominz, M.A., Browning, J.V., Miller, K.G., Sugarman, P.J., Mizintseva, S., Scotese, C.R.: Late Cretaceous to Miocene sea-level estimates from the New Jersey and Delaware coastal plain coreholes: an error analysis. Basin Research 20, 211–226, 2008.
Krantz, D.E., Williams, D.F., Jones, D.S.: Ecological and paleoenvironmental information using stable isotope profiles from living and fossil molluscs. Palaeogeography, Palaeoclimatology, Palaeoecology 58, 249–266. https://doi.org/10.1016/0031-0182(87)90064-2, 1987.
Kuznetsov, A.B., Semikhatov, M.A., Gorokhov, I.M.: The Sr isotope composition of the world ocean, marginal and inland seas: Implications for the Sr isotope stratigraphy. Stratigr. Geol. Correl. 20, 501–515. https://doi.org/10.1134/S0869593812060044, 2012.
Lartaud, F., Emmanuel, L., De Rafélis, M., Ropert, M., Labourdette, N., Richardson, C.A., Renard, M.: A latitudinal gradient of seasonal temperature variation recorded in oyster shells from the coastal waters of France and The Netherlands. Facies 56, 13, 2010.
Lear, C.H., Elderfield, H., Wilson, P.A.: A Cenozoic seawater Sr/Ca record from benthic foraminiferal calcite and its application in determining global weathering fluxes. Earth and Planetary Science Letters 208, 69–84. https://doi.org/10.1016/S0012-821X(02)01156-1, 2003.
Locarnini, R.A., Mishonov, A.V., Antonov, J.I., Boyer, T.P., Garcia, H.E., Baranova, O.K., Zweng, M.M., Paver, C.R., Reagan, J.R., Johnson, D.R., Hamilton, M., Seidov, D.: World ocean atlas 2013. Volume 1, Temperature. U.S. Department of Commerce, National Oceanic and Atmospheric Administration, National Environmental Satellite, Data and Information Service. https://doi.org/10.7289/v55x26vd, 2013.
Lorrain, A., Gillikin, D.P., Paulet, Y.-M., Chauvaud, L., Le Mercier, A., Navez, J., André, L.: Strong kinetic effects on Sr/Ca ratios in the calcitic bivalve *Pecten maximus*. Geology 33, 965–968, 2005.
Lorrain, A., Paulet, Y.-M., Chauvaud, L., Dunbar, R., Mucciarone, D., Fontugne, M.: $\delta^{13}C$ variation in scallop shells: increasing metabolic carbon contribution with body size? Geochimica et Cosmochimica Acta 68, 3509–3519, 2004.
Lowenstam, H.A., Epstein, S.: Paleotemperatures of the post-Aptian Cretaceous as determined by the oxygen isotope method. The Journal of Geology 62, 207–248, 1954.
MacDonald, B.A., Thompson, R.J.: Influence of temperature and food availability on the ecological energetics of the giant scallop *Placopecten magellanicus*. I. Growth rates of shell and somatic tissue. Marine ecology progress series. Oldendorf 25, 279–294, 1985.
McArthur, J.M., Howarth, R.J., Bailey, T.R.: Strontium Isotope Stratigraphy: LOWESS Version 3: Best Fit to the Marine Sr-Isotope Curve for 0–509 Ma and Accompanying Look-up Table for Deriving Numerical Age. The Journal of Geology 109, 155–170. https://doi.org/10.1086/319243, 2001.
McArthur, J.M., Steuber, T., Page, K.N., Landman, N.H.: Sr-isotope stratigraphy: assigning time in the Campanian, Pliensbachian, Toarcian, and Valanginian. The Journal of Geology 124, 569–586, 2016.

https://doi.org/10.5194/bg-2019-74
Preprint. Discussion started: 25 September 2019

1089 McConnaughey, T.A.: Sub-equilibrium oxygen-18 and carbon-13 levels in biological carbonates: carbonate and kinetic models.
1090 Coral Reefs 22, 316–327, 2003.
1091 McConnaughey, T.A., Burdett, J., Whelan, J.F., Paull, C.K.: Carbon isotopes in biological carbonates: respiration and
1092 photosynthesis. Geochimica et Cosmochimica Acta 61, 611–622, 1997.
1093 McConnaughey, T.A., Gillikin, D.P.: Carbon isotopes in mollusk shell carbonates. Geo-Marine Letters 28, 287–299.
1094 https://doi.org/10.1007/s00367-008-0116-4, 2008.
1095 Meyers, S.R., Malinverno, A.: Proterozoic Milankovitch cycles and the history of the solar system. PNAS 201717689.
1096 https://doi.org/10.1073/pnas.1717689115, 2018.
1097 Miller, K.G., Wright, J.D., Browning, J.V.: Visions of ice sheets in a greenhouse world. Marine Geology, Ocean Chemistry over the
1098 Phanerozoic and its links to Geological Processes 217, 215–231. https://doi.org/10.1016/j.margeo.2005.02.007, 2005.
1099 Misra, S., Froelich, P.N.: Lithium Isotope History of Cenozoic Seawater: Changes in Silicate Weathering and Reverse Weathering.
1100 Science 335, 818–823. https://doi.org/10.1126/science.1214697, 2012.
1101 Montgomery, P., Hailwood, E.A., Gale, A.S., Burnett, J.A.: The magnetostratigraphy of Coniacian-Late Campanian chalk sequences
1102 in southern England. Earth and Planetary Science Letters 156, 209–224. https://doi.org/10.1016/S0012-821X(98)00008-9, 1998.
1103 Mook, W.G.: Paleotemperatures and chlorinities from stable carbon and oxygen isotopes in shell carbonate. Palaeogeography,
1104 Palaeoclimatology, Palaeoecology 9, 245–263. https://doi.org/10.1016/0031-0182(71)90002-2, 1971.
1105 Mouchi, V., De Rafélis, M., Lartaud, F., Fialin, M., Verrecchia, E.: Chemical labelling of oyster shells used for time-calibrated high-
1106 resolution Mg/Ca ratios: a tool for estimation of past seasonal temperature variations. Palaeogeography, Palaeoclimatology,
1107 Palaeoecology 373, 66–74, 2013.
1108 NOAA Earth System Research Laboratory: NOAA Optimum Interpolation (IO) Sea Surface Temperature (SST)
1109 http://www.esrl.noaa.gov/psd/data/gridded/data.noaa.oisst.v2.html (accessed 01/21/19).
1110 Ogg, J.G., Ogg, G., Gradstein, F.M.: A concise geologic time scale: 2016. Elsevier, 2016.
1111 Palmer, M.R., Edmond, J.M.: The strontium isotope budget of the modern ocean. Earth and Planetary Science Letters 92, 11–26.
1112 https://doi.org/10.1016/0012-821X(89)90017-4, 1989.
1113 Palmer, R.E., Carriker, M.R.: Effects of cultural conditions on morphology of the shell of the oyster *Crassostrea virginica*, in:
1114 Proceedings of the National Shellfisheries Association. pp. 58–72, 1979.
1115 Pearson, P.N., Ditchfield, P.W., Singano, J., Harcourt-Brown, K.G., Nicholas, C.J., Olsson, R.K., Shackleton, N.J., Hall, M.A.: Warm
1116 tropical sea surface temperatures in the Late Cretaceous and Eocene epochs. Nature 413, 481, 2001.
1117 Perdiou, A., Thibault, N., Anderskouv, K., Van Buchem, F., Buijs, G.J.A., Bjerrum, C.J.: Orbital calibration of the late Campanian
1118 carbon isotope event in the North Sea. Journal of the Geological Society 173, 504–517, 2016.
1119 Prandle, D., Lane, A.: The annual temperature cycle in shelf seas. Continental Shelf Research 15, 681–704.
1120 https://doi.org/10.1016/0278-4343(94)E0029-L, 1995.
1121 R Core Team: R: A language and environment for statistical computing. R Foundation for Statistical Computing. Vienna, Austria,
1122 2013.
1123 Rausch, S., Böhm, F., Bach, W., Klügel, A., Eisenhauer, A.: Calcium carbonate veins in ocean crust record a threefold increase of
1124 seawater Mg/Ca in the past 30 million years. Earth and Planetary Science Letters 362, 215–224, 2013.
1125 Rayner, N.A., Parker, D.E., Horton, E.B., Folland, C.K., Alexander, L.V., Rowell, D.P., Kent, E.C., Kaplan, A.: Global analyses of sea
1126 surface temperature, sea ice, and night marine air temperature since the late nineteenth century. Journal of Geophysical
1127 Research: Atmospheres 108. https://doi.org/10.1029/2002JD002670, 2003.
1128 Reid, R.E.H.: The Chalk Sea. The Irish Naturalists' Journal 17, 357–375, 1973.
1129 Richardson, C.A., Peharda, M., Kennedy, H., Kennedy, P., Onofri, V.: Age, growth rate and season of recruitment of *Pinna nobilis*
1130 (L) in the Croatian Adriatic determined from Mg: Ca and Sr: Ca shell profiles. Journal of Experimental Marine Biology and
1131 Ecology 299, 1–16, 2004.
1132 Rothschild, B.J., Ault, J.S., Goulletquer, P., Heral, M.: Decline of the Chesapeake Bay oyster population: a century of habitat
1133 destruction and overfishing. Marine Ecology Progress Series 29–39, 1994.
1134 Roy, K., Jablonski, D., Martien, K.K.: Invariant size–frequency distributions along a latitudinal gradient in marine bivalves. PNAS 97,
1135 13150–13155. https://doi.org/10.1073/pnas.97.24.13150, 2000.
1136 Rucker, J.B., Valentine, J.W.: Salinity Response of Trace Element Concentration in *Crassostrea virginica*. Nature 190, 1099–1100.
1137 https://doi.org/10.1038/1901099a0, 1961.
1138 Sano, Y., Kobayashi, S., Shirai, K., Takahata, N., Matsumoto, K., Watanabe, T., Sowa, K., Iwai, K.: Past daily light cycle recorded in
1139 the strontium/calcium ratios of giant clam shells. Nat Commun 3, 761. https://doi.org/10.1038/ncomms1763, 2012.
1140 Schöne, B.R., Gillikin, D.P.: Unraveling environmental histories from skeletal diaries — Advances in sclerochronology.
1141 Palaeogeography, Palaeoclimatology, Palaeoecology, Unraveling environmental histories from skeletal diaries - advances in
1142 sclerochronology 373, 1–5. https://doi.org/10.1016/j.palaeo.2012.11.026, 2013.
1143 SCHÖNE, B.R., Houk, S.D., FREYRE CASTRO, A.D., Fiebig, J., Oschmann, W., KRÖNCKE, I., Dreyer, W., Gosselck, F.: Daily
1144 growth rates in shells of *Arctica islandica*: assessing sub-seasonal environmental controls on a long-lived bivalve mollusk.
1145 Palaios 20, 78–92, 2005.
1146 Schöne, B.R., Radermacher, P., Zhang, Z., Jacob, D.E.: Crystal fabrics and element impurities (Sr/Ca, Mg/Ca, and Ba/Ca) in shells
1147 of *Arctica islandica*—Implications for paleoclimate reconstructions. Palaeogeography, Palaeoclimatology, Palaeoecology 373,
1148 50–59, 2013.
1149 Schöne, B.R., Zhang, Z., Jacob, D., Gillikin, D.P., Tütken, T., Garbe-Schönberg, D., McConnaughey, T., Soldati, A.: Effect of
1150 organic matrices on the determination of the trace element chemistry (Mg, Sr, Mg/Ca, Sr/Ca) of aragonitic bivalve shells (*Arctica*
1151 *islandica*)—Comparison of ICP-OES and LA-ICP-MS data. Geochemical Journal 44, 23–37, 2010.
1152 Schöne, B.R., Zhang, Z., Radermacher, P., Thébault, J., Jacob, D.E., Nunn, E.V., Maurer, A.-F.: Sr/Ca and Mg/Ca ratios of
1153 ontogenetically old, long-lived bivalve shells (*Arctica islandica*) and their function as paleotemperature proxies.
1154 Palaeogeography, Palaeoclimatology, Palaeoecology 302, 52–64, 2011.
1155 Scotese, C.: A new global temperature curve for the Phanerozoic. Presented at the GSA Annual Meeting in Denver, Colorado, USA
1156 - 2016. https://doi.org/10.1130/abs/2016AM-287167, 2016

Snoeck, C., Lee-Thorp, J., Schulting, R., Jong, J., Debouge, W., Mattielli, N.: Calcined bone provides a reliable substrate for strontium isotope ratios as shown by an enrichment experiment. Rapid communications in mass spectrometry 29, 107–114, 2015.

Sørensen, A.M., Surlyk, F., Jagt, J.W.M.: Adaptive morphologies and guild structure in a high-diversity bivalve fauna from an early Campanian rocky shore, Ivö Klack (Sweden). Cretaceous Research 33, 21–41. https://doi.org/10.1016/j.cretres.2011.07.004, 2012.

Sørensen, A.M., Ullmann, C.V., Thibault, N., Korte, C.: Geochemical signatures of the early Campanian belemnite *Belemnellocamax mammillatus* from the Kristianstad Basin in Scania, Sweden. Palaeogeography, palaeoclimatology, palaeoecology 433, 191–200, 2015.

Stanley, S.M., Hardie, L.A.: Secular oscillations in the carbonate mineralogy of reef-building and sediment-producing organisms driven by tectonically forced shifts in seawater chemistry. Palaeogeography, Palaeoclimatology, Palaeoecology 144, 3–19, 1998.

Stenzel, H.B.: Aragonite and calcite as constituents of adult oyster shells. Science 142, 232–233, 1963.

Steuber, T.: Isotopic and chemical intra-shell variations in low-Mg calcite of rudist bivalves (Mollusca-Hippuritacea): disequilibrium fractionations and late Cretaceous seasonality. International Journal of Earth Sciences 88, 551–570, 1999.

Steuber, T., Rauch, M., Masse, J.-P., Graaf, J., Malkoč, M.: Low-latitude seasonality of Cretaceous temperatures in warm and cold episodes. Nature 437, 1341–1344, 2005.

Steuber, T., Veizer, J.: Phanerozoic record of plate tectonic control of seawater chemistry and carbonate sedimentation. Geology 30, 1123–1126. https://doi.org/10.1130/0091-7613(2002)030<1123:PROPTC>2.0.CO;2, 2002.

Strahl, J., Philipp, E., Brey, T., Broeg, K., Abele, D.: Physiological aging in the Icelandic population of the ocean quahog *Arctica islandica*. Aquatic Biology 1, 77–83, 2007.

Surge, D., Lohmann, K.C.: Evaluating Mg/Ca ratios as a temperature proxy in the estuarine oyster, *Crassostrea virginica*. Journal of Geophysical Research: Biogeosciences 113, 2008.

Surge, D., Lohmann, K.C., Dettman, D.L.: Controls on isotopic chemistry of the American oyster, *Crassostrea virginica*: implications for growth patterns. Palaeogeography, Palaeoclimatology, Palaeoecology 172, 283–296, 2001.

Surge, D.M., Lohmann, K.C., Goodfriend, G.A.: Reconstructing estuarine conditions: oyster shells as recorders of environmental change, Southwest Florida. Estuarine, Coastal and Shelf Science 57, 737–756. https://doi.org/10.1016/S0272-7714(02)00370-0, 2003.

Surlyk, F., Christensen, W.K.: Epifaunal zonation on an Upper Cretaceous rocky coast. Geology 2, 529–534, 1974.

Surlyk, F., Sørensen, A.M.: An early Campanian rocky shore at Ivö Klack, southern Sweden. Cretaceous Research 31, 567–576, 2010.

Thibault, N., Harlou, R., Schovsbo, N.H., Stemmerik, L., Surlyk, F.: Late Cretaceous (late Campanian–Maastrichtian) sea-surface temperature record of the Boreal Chalk Sea. Climate of the Past 12, 429–438, 2016.

Thibault, N., Husson, D., Harlou, R., Gardin, S., Galbrun, B., Huret, E., Minoletti, F.: Astronomical calibration of upper Campanian–Maastrichtian carbon isotope events and calcareous plankton biostratigraphy in the Indian Ocean (ODP Hole 762C): Implication for the age of the Campanian–Maastrichtian boundary. Palaeogeography, Palaeoclimatology, Palaeoecology 337–338, 52–71. https://doi.org/10.1016/j.palaeo.2012.03.027, 2012.

Ullmann, C.V., Böhm, F., Rickaby, R.E., Wiechert, U., Korte, C.: The Giant Pacific Oyster (*Crassostrea gigas*) as a modern analog for fossil ostreoids: isotopic (Ca, O, C) and elemental (Mg/Ca, Sr/Ca, Mn/Ca) proxies. Geochemistry, Geophysics, Geosystems 14, 4109–4120, 2013.

Ullmann, C.V., Korte, C.: Diagenetic alteration in low-Mg calcite from macrofossils: a review. Geological Quarterly 59, 3–20, 2015.

Ullmann, C.V., Wiechert, U., Korte, C.: Oxygen isotope fluctuations in a modern North Sea oyster (*Crassostrea gigas*) compared with annual variations in seawater temperature: Implications for palaeoclimate studies. Chemical Geology 277, 160–166, 2010.

Upchurch Jr, G.R., Kiehl, J., Shields, C., Scherer, J., Scotese, C.: Latitudinal temperature gradients and high-latitude temperatures during the latest Cretaceous: Congruence of geologic data and climate models. Geology 43, 683–686, 2015.

Vansteenberge, S., de Winter, N.J., Sinnesael, M., Xueqin, Z., Verheyden, S., Claeys, P. Benchtop µXRF as a tool for speleothem trace elemental analysis: validation, limitations and application to an Eemian to early Weichselian (125-97 Ma) stalagmite from Belgium. Palaeogeography, Palaeoclimatology, Palaeoecology, in review.

Veizer, J.: Chemical diagenesis of carbonates: theory and application of trace element technique, 1983.

Voigt, S., Friedrich, O., Norris, R.D., Schönfeld, J.: Campanian–Maastrichtian carbon isotope stratigraphy: shelf-ocean correlation between the European shelf sea and the tropical Pacific Ocean. Newsletters on Stratigraphy 44, 57–72, 2010.

Voigt, S., Schönfeld, J.: Cyclostratigraphy of the reference section for the Cretaceous white chalk of northern Germany, Lägerdorf–Kronsmoor: A late Campanian–early Maastrichtian orbital time scale. Palaeogeography, Palaeoclimatology, Palaeoecology 287, 67–80. https://doi.org/10.1016/j.palaeo.2010.01.017, 2010.

Von Bertalanffy, L.: Quantitative laws in metabolism and growth. The quarterly review of biology 32, 217–231, 1957.

Wagreich, M., Hohenegger, J., Neuhuber, S.: Nannofossil biostratigraphy, strontium and carbon isotope stratigraphy, cyclostratigraphy and an astronomically calibrated duration of the Late Campanian *Radotruncana calcarata* Zone. Cretaceous Research 38, 80–96, 2012.

Warter, V., Erez, J., Müller, W.: Environmental and physiological controls on daily trace element incorporation in *Tridacna crocea* from combined laboratory culturing and ultra-high resolution LA-ICP-MS analysis. Palaeogeography, Palaeoclimatology, Palaeoecology 496, 32–47. https://doi.org/10.1016/j.palaeo.2017.12.038, 2018.

Watanabe, T., Suzuki, A., Kawahata, H., Kan, H., Ogawa, S.: A 60-year isotopic record from a mid-Holocene fossil giant clam (*Tridacna gigas*) in the Ryukyu Islands: physiological and paleoclimatic implications. Palaeogeography, Palaeoclimatology, Palaeoecology 212, 343–354, 2004.

Weiner, S., Dove, P.M.: An overview of biomineralization processes and the problem of the vital effect. Reviews in mineralogy and geochemistry 54, 1–29, 2003.

Weis, D., Kieffer, B., Maerschalk, C., Barling, J., Jong, J. de, Williams, G.A., Hanano, D., Pretorius, W., Mattielli, N., Scoates, J.S., Goolaerts, A., Friedman, R.M., Mahoney, J.B.: High-precision isotopic characterization of USGS reference materials by TIMS and MC-ICP-MS. Geochemistry, Geophysics, Geosystems 7, Q08006. https://doi.org/10.1029/2006GC001283, 2006.

https://doi.org/10.5194/bg-2019-74
Preprint. Discussion started: 25 September 2019

1226 Wendler, I.: A critical evaluation of carbon isotope stratigraphy and biostratigraphic implications for Late Cretaceous global
1227 correlation. Earth-Science Reviews 126, 116–146. https://doi.org/10.1016/j.earscirev.2013.08.003, 2013.
1228 Yang, D., Huang, Y., Guo, W., Huang, Q., Ren, Y., Wang, C.: Late Santonian-early Campanian lake-level fluctuations in the
1229 Songliao Basin, NE China and their relationship to coeval eustatic changes. Cretaceous Research 92, 138–149.
1230 https://doi.org/10.1016/j.cretres.2018.07.008, 2018.
1231 Yoshimura, T., Tanimizu, M., Inoue, M., Suzuki, A., Iwasaki, N., Kawahata, H.: Mg isotope fractionation in biogenic carbonates of
1232 deep-sea coral, benthic foraminifera, and hermatypic coral. Anal Bioanal Chem 401, 2755. https://doi.org/10.1007/s00216-011-
1233 5264-0, 2011.
1234 Zimmt, J.B., Lockwood, R., Andrus, C.F.T., Herbert, G.S.: Sclerochronological basis for growth band counting: A reliable technique
1235 for life-span determination of *Crassostrea virginica* from the mid-Atlantic United States. Palaeogeography, Palaeoclimatology,
1236 Palaeoecology 516, 54–63, 2018.